Accurate Determination of the Reaction Course in HY2 ⇋ Y+YH (Y = O, S): A Detailed Analysis of the Covalent- to Hydrogen-Bonding Transition.

ARTICLE *in* THE JOURNAL OF PHYSICAL CHEMISTRY A · APRIL 2013

Impact Factor: 2.69 · DOI: 10.1021/jp401384d · Source: PubMed

1 AUTHOR:

Antonio J. C. Varandas
University of Coimbra
382 PUBLICATIONS **6,749** CITATIONS

SEE PROFILE

THE JOURNAL OF PHYSICAL CHEMISTRY A

Article

pubs.acs.org/JPCA

Accurate Determination of the Reaction Course in $HY_2 \rightleftharpoons Y + YH$ (Y = O, S): Detailed Analysis of the Covalent- to Hydrogen-Bonding Transition

A. J. C. Varandas[†]

Departamento de Química, Universidade de Coimbra, 3004-535 Coimbra, Portugal

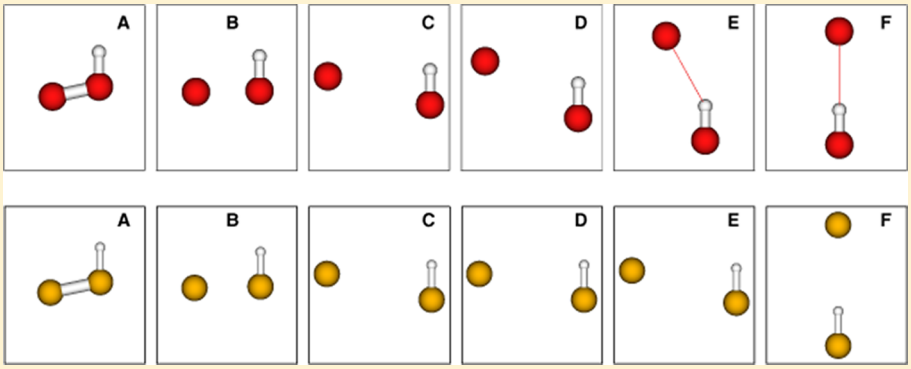

ABSTRACT: The accurate prediction of a bond-breaking/bond-forming reaction course is useful but very difficult. Toward this goal, a cost-effective multireference scheme (A. J. C. Varandas, *J. Chem. Theory Comput.* **2012**, *8*, 428) is tested that provides a generalization of the Hartree−Fock plus dispersion model for closed-shell interactions, and hence is based on the popular but largely untested idea of performing single point calculations with a high-level method at stationary points or along paths located using a lower level method. The energetics so calculated for the reaction $HO_2 \rightleftharpoons O + OH$ is predicted in excellent agreement with the experimental data, whereas the reaction path shows a scar at the onset of hydrogen-bonding: a weak van der Waals type minimum separated from the deep covalent well by a small barrier, all below the O + OH asymptote. The O−OH long-range interaction potential is also examined and possible implications in reaction dynamics discussed. Corresponding attributes for the reaction $HS_2 \rightleftharpoons S + SH$ are predicted, in good agreement with the best theoretical and experimental results. A perspective on the general utility of the approach is presented.

1. INTRODUCTION

Finding a reaction path (as well as any underlying first-order saddle point or transition state[1]) is a task of primary importance in reaction dynamics since the early stages of transition-state theory.[2] Many approaches have been introduced for this purpose, and the methods implemented in electronic structure codes for both semiempirical and ab initio calculations.[3−10] One of the most useful concepts emerging from that research is the one of intrinsic reaction coordinate (IRC): a mass-weighted steepest descent path starting from a first-order saddle point; the reader is addressed to the paper by Maeda and Morokuma[10] for recent developments.

An approach that has been used even prior to the appearance of the concept of IRC path consists of selecting a reaction coordinate and consider all others constrained or optimized in some manner. Unfortunately, some paths generated in this way may give rise to discontinuities.[4] The results may also be not free from some ambiguity as they depend upon the choice of coordinates (Cartesian, mass-weighted, internal coordinates, etc.) or even vary upon the sense of which direction the calculation progresses.[9] Thus, it may not be warranted that such paths go through the saddle point for reaction. However, the approach is simple to apply and particularly useful if a "well-defined" reaction coordinate is available or the aim is to establish an intuitive path leading to reaction but which, unlike IRC, does not satisfy Hamilton's equations of motion for an infinitely slow trajectory. Of particular relevance is the optimum reaction coordinate (ORC) path where all but the reactive coordinate (also called "inactive") are optimized. For example, if the accuracy of an ab initio scheme for electronic structure calculations is being tested, the ORC path may provide a kind of maximum error because the optimized coordinates can assume extreme differences in comparison with other schemes. Of course, likewise IRC, the ORC path may be forced to encompass a known stationary point such as a transition state. A first goal of the present paper is to put in perspective both ORC and IRC paths for unraveling potential energy surfaces (PESs), because a straight exploitation in their full dimensionality can be a formidable task at a high level of ab initio

Special Issue: Joel M. Bowman Festschrift

Received: February 7, 2013
Revised: March 29, 2013
Published: April 2, 2013

multireference theory even for systems like the ones here considered.

It should be stated from the outset that the idea of calculating a reaction path by combining feasible methodologies is not new. In fact, it is so conventional that even notations for doing so are common in the literature to prepare input files for use in electronic structure packages. What is missing is convincing evidence on how such combinations work or under which conditions a given selection of methods works and where it must be replaced by more rigorous schemes. Thus, any agreement with more rigorous calculations may be mere coincidence. Indeed, it is not uncommon to find work on reaction paths utilizing single-reference methods even though it is conventional wisdom that the wave function is multireference. A second purpose of this paper is then to show that ORC or IRC paths calculated at the relatively modest complete-active-space SCF (or CASSCF) level of theory followed by single-point multireference configuration interaction[11] (MRCI) calculations can provide highly accurate curves when compared with the essentially unaffordable, directly optimized, MRCI ones. Rather than novelty, the present in depth analysis hopes to elucidate the reader about the accuracy of the proposed scheme, because MRCI optimizations can here be performed. Due to computational cost, only two systems will be investigated (see also elsewhere[12]), but untested cases and potential difficulties will also be put in perspective.

With a focus on relatively small polyatomics where the targeted theoretical methods may be viable, we discuss in the theory section a reliable ab initio strategy to uncover the details of a bond-breaking/bond-forming reaction path. Use will then follow in the case studies section. As a try-out, we will first examine in detail the hydroperoxyl radical, a species known to play a key role in planetary atmospheres[13] and interstellar clouds.[14−16] The methodology is next applied to the disulfanyl radical or thiosulfeno (HS_2), the second-row analogue of HO_2. Because both the title radicals form an important group of reactive intermediates, it is our third purpose in this paper to report what is perhaps the most accurate data so far available for some of their attributes which, in the case of HS_2, are partly unknown. A brief synopsis is therefore justified at this point.

The hydroperoxyl radical is key in Earth's atmosphere where it participates on the removal of stratospheric "odd-oxygen" through the highly exothermic and barrier-free reaction $O(^3P) + OH(X\ ^2\Pi) \rightleftharpoons HO_2^\star \rightarrow H + O_2(X^3\Sigma_g^-)$, and of high-vibrationally excited mesospheric OH.[13] It is also a source of O_2 even in ultracold regimes,[14] with much interest attracted due to the so-called interstellar "oxygen problem":[17] measurements[18] suggest its abundance in the cores of the interstellar clouds to be orders of magnitude lower than predicted by the latest astrochemical models.[19] A possible cause of uncertainty is the low-temperature rate constant of the above reaction, which has not been accurately determined.[19] Crucial for theoretical work is the potential-energy surface (PES) for the X^2A'' ground electronic state of HO_2, which has been investigated at various levels of ab initio theory.[20−35] Calculations cover from bound vibrational states and resonances[36−43] to reactive scattering using both time-independent and time-dependent methods.[36,44−55] Most such studies employed one of the three following PESs: Melius−Blint,[20] double many-body expansion (DMBE IV[30]), and diatomics-in-molecules (DIM).[31] Although DMBE IV is likely the most widely used for dynamics studies due to appearing remarkably adequate[56] for calculating reaction rate constants, there has been recently much interest on the so-called XXZLG[57] PES, the latest version[58] of which represents a spline interpolant to about 18 000 MRCI + Q points calculated with an augmented quadruple-ζ correlation consistent basis set (AVQZ) of the Dunning[59−61] type and the Davidson correction. In fact, theoretical investigations of the O + OH rate constant below 50 K have utilized either XXZLG or both this and the DMBE IV PESs;[15,16,56,62−65] a review[66] on complex-forming reactions, and an application of the O + OH rate constants[67] calculated with DMBE IV in modeling the hydroxyl nightglow in the atmosphere[68] have also appeared. Because accurate ab initio energies are computationally heavy, there is a great demand for cost-effective methods that retain a high reliability. We will use an approach that we have recently[12] suggested and applied to the reaction $OH + O_2 \rightleftharpoons HO_3$ (but conceivably utilized in various related forms by others), because a double-check with MRCI calculations is here possible.

The second case study is the second-row congener $HS_2 \rightleftharpoons S + SH$. Because a MRCI-based PES, suitably CBS extrapolated using the AV(X+d)Z (X = T, Q) basis (i.e., the standard[69] AVXZ one plus core-polarization high-exponent d functions for S and AVXZ for H) has been reported[70] for the disulfanyl radical from DMBE[71,72] theory, the reader is there directed for details on previous work.[73−81] Briefly, ab initio studies[77−82] covered both structural and vibrational information on the ground and excited states of HS_2 mostly with single-reference coupled-cluster (CC) methods such as CCSD(T) and density functional theory (DFT). Structural and energetic properties of HS_2 and the $HSS \rightleftharpoons SSH$ transition state have also been examined,[80] whereas Peterson et al.[81] reported calculations of the equilibrium geometry for the ground and first excited states of HS_2 with CC methods followed by extrapolation. Suffice it to add that the results here reported demand a level of detail that could hardly be achieved by the above global PES.[70] Thus our qualification[70] of high accuracy may still be valid, but the implications of some subtleties here predicted cannot presently be assessed.

2. CASDC SCHEME

A general and most convenient partition of the molecular energy consists of writing

$$E = E_{CAS}(\mathbf{R}) + E_{dc}(\mathbf{R}) \quad (1)$$

where CAS is an abbreviation of complete-active-space SCF (CASSCF), and dc labels the dynamical correlation; **R** is the vector of the nuclear coordinates. The former energy component is known to be system specific and accounts for the nondynamical correlation, which allows us to describe degeneracies and near-degeneracies of the molecular orbitals: it is particularly critical near crossings, near avoided-crossings, and close to dissociation asymptotes. In turn, the dynamical correlation is physical in the sense that it matches the long-range energy associated with the dispersion forces. Thus, the CASSCF energy accounts for the valence forces and includes any long-range contributions that arise due to the electrostatic interaction of permanent electrostatic moments and induction-type contributions: it is then expected to manifest a strong dependence on the orientation of the interacting partners. Conversely, the dc energy should show a small directional dependence. Thus, the optimized reaction path should be mostly dictated by the energy contributions calculated at the CASSCF level of theory, except for the energy itself, which must be more attractive due to the dynamical correlation term.

dx.doi.org/10.1021/jp401384d | J. Phys. Chem. A 2013, 117, 7393−7407

When the wave function is dominated by the Hartree−Fock term, as is commonly the case for closed-shell interactions, eq 1 reduces to the well-known sum of the Hartree−Fock plus dynamical (total) correlation. If the latter is then approximated by the dispersion energy suitably damped to account for electron-exchange and charge-overlap effects, one gets the popular Hartree−Fock plus damped dispersion[83] (HFD) model (an extension has recently been reported,[84] and an analog available[85] where the HF term is replaced by the first-order energy of exchange-perturbation theory).

The utilized computational strategy stems from the following four-point premise:[12]

1. Bond-breaking/bond-forming reactions are best treated by multireference methods such as MRCI, preferably when the Davidson correction (MRCI + Q) is added.
2. A convenient reference for MRCI is the full-valence-complete-active-space (FVCAS) wave function, warranting in principle a correct description at dissociation.
3. Such processes can be described by a single reactive coordinate.
4. Single-point MRCI + Q calculations along the optimized FVCAS path should differ marginally from the unaffordable directly optimized MRCI + Q ones.

Hereinafter this is referred to as CASDC to imply that it is based on the sum of the optimized CASSCF energy plus the dynamical correlation calculated pointwise, i.e., in close analogy with the HFD[83] model for closed-shell interactions. The acronym CASDC will then replace the somewhat less clear denomination of opt-CAS employed elsewhere.[12]

As noted above, the idea of performing single-point MRCI + Q calculations along the optimized FVCAS path (or any other obtained with a lower level method) is common in computational chemistry. Indeed, composite procedures are popular[86] in the field, with notations such as CCSD(T)/AVTZ//B3LYP/6-31G* being conventional to indicate CCSD(T) calculations at a geometry or along a DFT optimized path. Such schemes follow from the observation that the geometry is often less sensitive to the theoretical level than relative energies. Note that most such models are single-reference based and rely on the fact that effects from extending the basis are to a certain degree additive. However, there is no good reason for assuming that the considerations above apply, in particular for the adequacy of obtaining at the single-reference level of theory the geometries where higher-level single-point calculations are to be performed. This should be particularly so when dealing with open-shell reactive systems, as is here the case. Because the chosen low-level theory plays a key role in predicting a geometry or path as close as possible to the "true" one, the present choice of a CASSCF wave function may then play a key role, with the selection above usually providing a good compromise for accuracy and affordability. We emphasize that the use of CASSCF methodology has a tradition[35,87] (and references therein) to characterize the PESs of reactive species, but not quite in the context here reported. Similarly, the notation MRCI + Q/AVTZ//CASSCF/AVTZ could be utilized, although we adopt CASDC for two reasons: first, for brevity, and then to parallel HFD where the above considerations apply in a corresponding manner (the HF wave function should then be as close as possible to its limit); second, because both theories used in CASDC are multi-reference-type and complementary in the sense that the high-level theory attempts to recover the dc that lacks in the low-level one. This is unique among all composite schemes. Of course, one could think of estimating the dynamical correlation more cost-effectively, e.g., with multireference many-body perturbation theory.[11] Such a possibility will be of no concern in the present work. A further remark is to note that other definitions of reaction path (including IRC) could be adopted, although we use mostly the simplest one (ORC). In fact, there should be no difficulty in generalizing the scheme to other paths as long as they describe the envisaged bond-breaking/bond-forming process.

3. RESULTS AND DISCUSSION

Calculations have been carried out for the HY_aY_b (Y = O, S) radicals at the CASSCF level of theory along the coordinate (Y_aY_b) chosen to define the bond-breaking/bond-forming reaction, with all other degrees of freedom optimized at each point of the predefined grid; *a* and *b* label the Y atoms. In both cases, an atomic basis set of the cc-pVXZ type[59,69,88] has been utilized. For HO_2, extra functions designed to include core−core and core−valence correlations have been added to the correlation-consistent basis whereas, for HS_2, extra high-exponent d functions have been used: CVXZ and V(X+d)Z, respectively. Although a more flexible basis would have been desirable when the long-range part of the PESs was explored, the present choice has been judged as a good compromise given the high quality of the results previously obtained for HO_3 and the interest in treating core effects at the valence regions of HO_2. Our choice seems to be validated by further calculations carried out for HO_2 and HS_2 with the aug-cc-VXZ and aug-cc-V(X+d)Z basis [AVXZ and AV(X+d)Z], respectively, which contain diffuse orbitals. MRCI + Q calculations were next performed at each point of the optimized grid. Because we have already emphasized[12] the importance of the Davidson correction, it will not be repeated here. Suffice it to recall that any truncated CI-method suffers from lack of size extensivity,[11] and hence the need to mitigate such a deficiency; see elsewhere[89] for a review of the latest developments in the ab initio CI methodology.

Specifically, MRCI calculations have been done for O_aO_b distances varying from 1.2 to 100 Å, with the latter taken as the asymptote for separated products. All have employed the internally contracted MRCI[90,91] method as implemented in Molpro.[92] They involved 6 states with all (11) molecular orbitals considered as active, yielding 5445 configuration-state functions (CSFs) for the CASSCF wave function. For affordability, 2 molecular orbitals have been considered to be closed and 9 active in the MRCI, yielding a total of 47 503 080 contracted configurations for the CV5Z basis. A large number of direct optimizations at the MRCI level, some followed by harmonic vibrational frequency and normal mode calculations, have also been done. Because they are extremely time demanding[93] even for a small basis, only CVDZ and CVTZ were employed. Except when indicated otherwise, and for the vdW attributes where a gradient as small as 1 μE_h $Å^{-1}$ is utilized, convergence thresholds were kept at the default values.[92]

For enhanced accuracy, the two contributions that make up the electronic energy in eq 1 have been separately extrapolated to the complete basis set (CBS) limit through a series of calculations carried out using a basis with cardinal numbers up to X = 6. For the CASSCF energy, adaptations[94] of the Karton−Martin[95,96] (KM) formulas have been employed to approximate the CBS limit. In turn, our uniform singlet- and

dx.doi.org/10.1021/jp401384d | J. Phys. Chem. A 2013, 117, 7393−7407

triplet-pair extrapolation[94] (USTE) protocol has been utilized for the dynamical correlation energy using the results for the basis with the two highest affordable cardinal numbers: typically CBS(Q,5), with CBS implying for HO_2 such a level of extrapolation unless specified otherwise. (T,Q) and a few (5,6) extrapolations have also been carried out to help define the error bar upon CBS extrapolation. Note that backward use of CBS(Q,5) yields a CVTZ dc energy that matches nicely the calculated value, thence validating the method. In fact, an asset of USTE is that it often allows reliable extrapolations even when X-pairs as small as (T,Q) [often (D,T)] are utilized.[94] Despite the basis selection, some core correlation effects had to be overlooked due to the computational burden. Contributions such as relativistic effects, diagonal Born−Oppenheimer, and spin−orbit corrections are expected to be small for light atoms, and hence have here been assumed to be negligible. This may find support on recent calculations for the related HO_3 radical[97] where they have been shown to be small. Additionally, the basis set superposition error,[98] which is known to plague supermolecular calculations has been ignored because both components of the total energy have been CBS extrapolated.[99−101]

A corresponding set of CASSCF and MRCI calculations were done for HS_2. They were carried out with no symmetry for 6 states (all equally weighted), first within the frozen-core (FC: 10 closed orbitals and 9 active ones) approximation, and then by considering all 19 molecular orbitals as active, yielding 92 055 CSFs for the CASSCF wave function. In standard notation,[86] this corresponds to a CASSCF[33,19] for a 33-electron system, heretofore labeled as NC (nonclosed orbitals). Of the 19 molecular orbitals, the lowest 4 were taken as core and 9 were considered as active in the MRCI, thus leaving closed the other 6. This yields a total of 9 986 376 contracted configurations for the V(T+d)Z basis. Although we have encountered some difficulty in converging the MRCI energy to the proper state beyond 9 Å, this is estimated to cause an error of <0.03 kcal mol^{-1} and so should not be of major concern. We advance that CASSCF calculations assuming the 1s, 2s, and 2p orbitals of S to be closed (FC) yield essentially the same location for the saddle point connecting the covalent to the vdW minimum as well as for the latter, but the energetics at the MRCI level shows some small differences. Except for extrapolations where cardinals up to X = 5 are used, most calculations employ the V(T+d)Z basis with convergence thresholds at least as demanding as the default in Molpro (typically 10^{-5} E_h $Å^{-1}$, and often smaller for the gradient).

3.1. Hydroperoxyl Radical. *3.1.1. Bond-Breaking/Bond-Forming Reaction Path.* Figure 1 compares the CASDC/CVXZ with the directly optimized MRCI/CVXZ ORC paths for HO_2, X = D, T. The two curves correspond therefore to optimizations of all coordinates, but the inactive one at each point of the predefined grid. For the CVTZ basis, the MRCI path has been calculated at a somewhat smaller number of geometries than for CVDZ, with the symbols in Figure 2 indicating the chosen geometries. As Figure 1 shows, the curves from both approaches are indistinguishable except for a narrow region where the transition from H-bonding to covalent-bonding occurs, which is characterized by a saddle point (see later). Such a transition between the two bonding regimes is best illustrated in Figure 3, which shows snapshots of the various structures involved as the reaction coordinate progresses toward dissociation (from the left- to the right-hand-side of the panel). Note the small wiggle in Figure 2 after

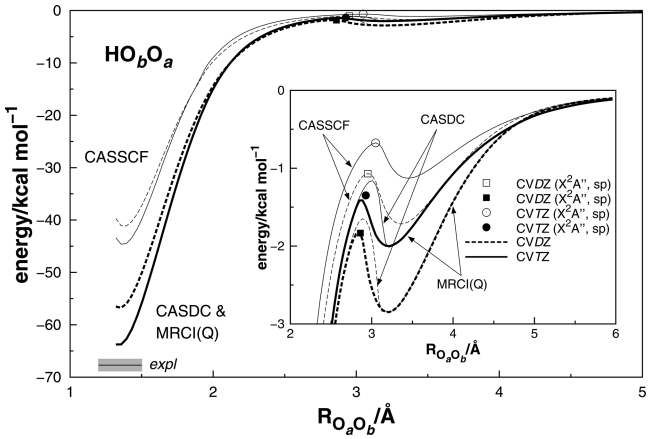

Figure 1. Optimal paths for the bond-breaking/bond-forming reaction HO_2 ⇌ O + OH: CASDC (thin lines, open symbols); directly optimized at MRCI + Q level of theory (dark lines, solid symbols) with same basis. Also indicated are the calculated saddle points and the experimental data whose averaged value is indicated by the small line segment between 1.2 and 1.5 Å. The reference corresponds to the energy of the separated fragments. Note that the CASDC and MRCI + Q curves are essentially indistinguishable but for the region in the inset (see the text).

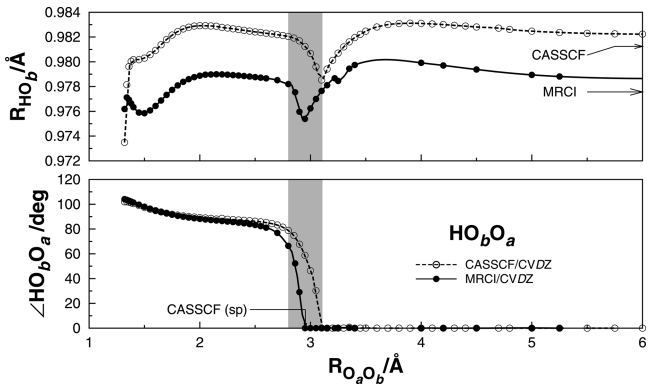

Figure 2. Optimized coordinates along the reaction path. The shaded area delimits the covalent ⇌ H-bond transition region centered at the CASSCF saddle point (margins separated by ±0.15 $Å^{-1}$ for both sides). Also signaled is the corresponding OH equilibrium distance which, at 100 Å, agrees within a few per ten thousand of Å with that obtained for the supermolecule.

3 Å, which may reflect some noise due to the use of small, yet finite, values for numerical convergence. Furthermore, Figure 1 shows that the good agreement extends beyond the vdW minimum (where the optimum value of ∠HO_bO_a is equal to zero within the numerical error), very much in line with the results of the HFD model for closed-shell interactions.

Excluding therefore a narrow region ($2.8 \le R_{O_aO_b}/Å \le 3.1$) where proper optimization of geometry can be somewhat precarious and costly, the average root mean squared deviation (rmsd) over 40 points is only of 12.5 cm^{-1} for the CVDZ basis (11.5 cm^{-1} for the 34 calculated CVTZ points, excluding the transition region). Such small values can be understood from the near parallelism of the optimized CASSCF and MRCI curves for the OH bond distance (and to a less extent to the similarity of the valence angle, ∠HO_bO_a) in Figure 2; similarly shaped curves in a plot analogous to Figure 2 but with the apex in the shadded area of the top panel just slightly shifted to larger distances have been obtained for the CVTZ basis. It is

dx.doi.org/10.1021/jp401384d | J. Phys. Chem. A 2013, 117, 7393−7407

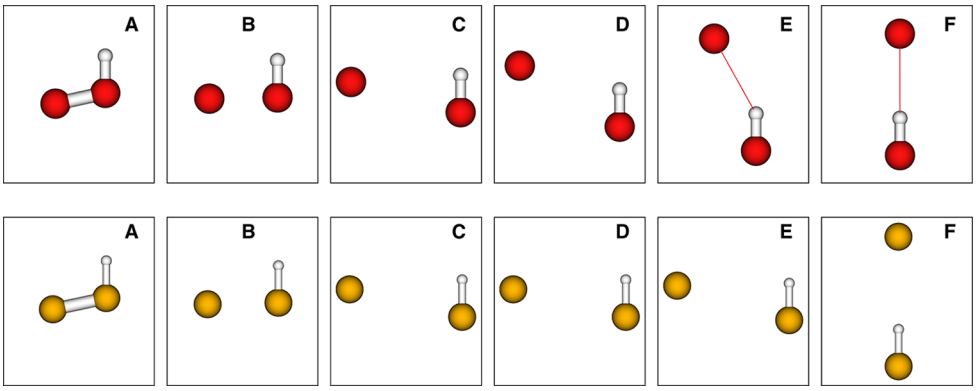

Figure 3. Reactions $HY_2 \rightarrow HY + Y$ (Y = O, S) at the CASSCF/CXZ (respectively, X = 5,T) level of theory as they progress from the covalent (panel A) to the vdW minima (F). In panels A–F (top) for HO_2, the reaction coordinate is of 1.34, 1.85, 3.00, 3.08, 3.15 (saddle point), and 3.24 Å. For HS_2 (bottom panels), the corresponding reaction coordinate as calculated at the FC level has the values of 2.0, 2.6, 4.2, 4.3, 4.43 (saddle point), and 4.8 Å in the same order. Note the fast change in orientation over the region where the binding character changes (see Figures 1 and 8, and text).

the above parallelism that is responsible for the high accuracy achieved by the CASDC scheme in describing the detailed energetics of this reaction. Not surprisingly, at the transition region encompassing 6 points, the deviations can reach up to ~200 cm^{-1} (still $\lesssim$1 mE_h), for the CVDZ and CVTZ basis when the simple ORC path is considered. Yet, e.g., for the CVDZ basis, the rmsd is still of only 16.2 cm^{-1}, which is due to the peaked nature the deviations at the saddle point region. So, the present results support the few[12] for HO_3 where CASDC deviations in bond lengths of $\ll$1% and bond angles of 2–4% have been observed.

The above discrepancy is best rationalized by calculating the optimum isomerization path, with the reaction coordinate for evolving from the $O_bH\cdots O_a$ (vdW minimum) to the HO_bO_a (covalent minimum) being now chosen to be $\angle HO_bO_a$. For brevity, only the CASSCF/CVDZ curve and the saddle point at the MRCI/CVDZ level of theory are calculated. The former has been obtained by optimizing the HO_b and O_aO_b bond lengths at the predefined grid of values taken to map $\angle HO_bO_a$. The results are shown in Figure 4. Similar trends are observed at both levels of theory except for the location of the saddle point that is slightly shifted to larger O_aO_b distances in the CASSCF case. Also shown for comparison in Figure 4 is the calculated IRC path, which connects the covalent and vdW minima. As seen, the ORC path includes by built-in construction the saddle point for reaction at the appropriate (CASSCF) level of theory, very much like the IRC path. Clearly, there is a close agreement between the ORC and IRC paths when a single channel dominates, with a sudden change occurring in the ORC path whenever an alternative, more favorable path, becomes accessible. Indeed, the optimized bending motion starting from the deep covalent minimum tends to lead to a blind valley via contraction of the OH bond before jumping to the exit channel where the vdW minimum occurs. This can be seen from Figure 4 or even more clearly from the contour plot of, e.g., Figure 3 of the DMBE IV paper,[30] an issue that has been left uncommented at the time of writing that paper. Of course, the above result bears no implication on the energetics of the overall reaction and it has only a mild influence on the detailed energetics along the reaction path. In fact, a comparison of two sets of electronic structure results for the ORC and IRC paths (not shown) suggests that the errors in the former may provide a kind of maximum error because fully optimized geometries (which are prone to show the largest energetic differences) can in principle be reached: the ORC path has no constraints such as in IRC where they are dictated by solving a differential equation. Indeed, this appears to be the case, with the IRC paths at the CASSCF and MRCI levels showing a closer parallelism in this troubling region than the corresponding ORC ones. We emphasize that the ORC and IRC paths lie close to each other whenever a single channel is open. This is also visible from Figure 4 if one realizes that $\angle HO_bO_a$ varies mostly in the saddle point region for isomerization.

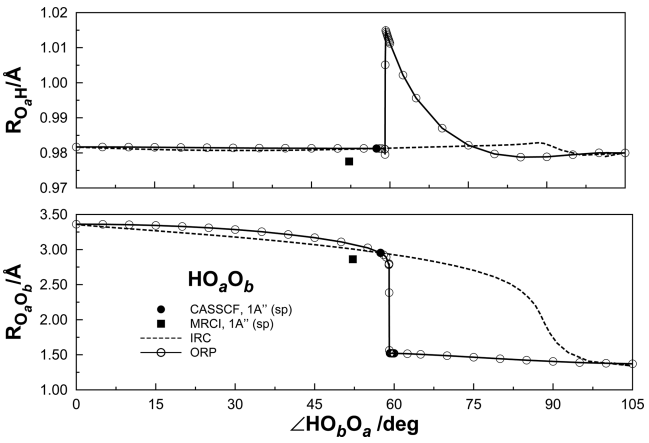

Figure 4. ORC as a function of the angle $\angle HO_bO_a$ at the CASSCF/CVDZ level of theory. Also shown are the calculated ORC points (open circles) and the saddle point, which have been estimated with a gradient of up to 1.0×10^{-5} E_h $Å^{-1}$ at both the CASSCF/CVDZ (solid circle) and MRCI/CVDZ (solid square) levels of theory.

3.1.2. Stationary Points. We begin this subsection with an accurate characterization of the stationary points that arise along the reaction path. Figure 5 illustrates the CASDC paths for larger basis as well as the CBS(Q,5) curve and a few CBS(5,6) points. All single-point MRCI calculations required for the extrapolations were carried out on the optimized CASSCF/CV5Z reaction path (this as well the optimal X = D, T ones are also shown in Figure 5 for comparison). The energetics and structural characterization of the deep chemical (covalent) and vdW minima are given in Figure 1, with the harmonic frequencies determined only at the above MRCI levels of theory. Due to being relatively inexpensive and

dx.doi.org/10.1021/jp401384d | J. Phys. Chem. A 2013, 117, 7393–7407

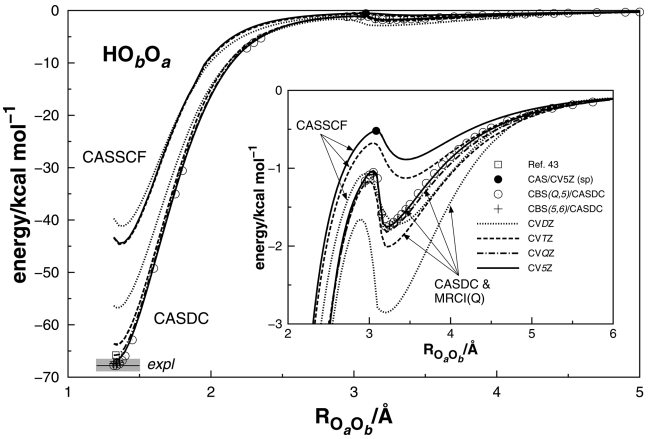

Figure 5. Optimized CASDC/CVXZ and CBS/CASDC/CVXZ reaction paths in $HO_2 \rightleftharpoons O + OH$; X = D, T, Q, 5, 6. Also shown are the optimal CASSCF/CVXZ (X = D, T, 5) paths, calculated saddle points, and CBS(Q,5) and CBS(5,6) energies (without spline fit); note that the energies can hardly be seen in the inset as they fall close to the CV5Z curve. The reference energy is as in Figure 1.

consensual, CASSCF energies will not be reported. Two observations should be made. First, the calculated dissociation energy, including the experimental[102,103] zero-point energy (ZPE) correction, is predicted at an unprecedented good agreement with the experimental counterpart: 64.5 ± 0.3 kcal mol^{-1} vs 64.7 ± 1.1 kcal mol^{-1}, respectively. Note that the error bar is estimated so as to encompass the various CBS predictions: 64.48 kcal mol^{-1} at CBS(T,Q), 64.74 kcal mol^{-1} at CBS(Q,5), and 64.39 kcal mol^{-1} at CBS(5,6). In turn, the experimental value represents an average that embraces the two available estimates.[104,105] Note that the equilibrium geometry is given only at the CBS(Q,5) level as only three geometries near the covalent minimum were considered for the CBS(5,6) extrapolation. Nevertheless, the result obtained seems to agree with the tabulated one[106] up to about ±0.001 Å.

The second notable observation refers to the "scar" that arises in the region where the interaction changes from dictated by the strong dipole−quadrupole OH···O interaction (plus higher-order electrostatic contributions as well as the less directional induction and dispersion ones) to a covalent interaction (Figure 3). This feature, which may be rationalized as arising from the mixing of configurations pertaining to those two regimes, has been discussed in detail[12,107] for the related (naturally more complicated) $HO_3 \rightleftharpoons O_2 + OH$ reaction and hence no further analysis is here deemed to be necessary. Suffice it to add that a similar topographical attribute has been the object of intensive study for the $O(^3P) + O_2$ reaction;[108] the van der Waals (vdW) attraction is in this case due mostly to the electrostatic quadrupole−quadrupole and dispersion forces. Indeed, such a feature is likely to be more common than anticipated.[12] Although reasonably sharp extrema arise as a consequence of the issues discussed at the end of the previous subsection, there are no discontinuities at the CASDC level of theory. Note from Figure 1 that the MRCI/CVTZ saddle point does not fall over the MRCI + Q/CVTZ curve, which may be

Table 1. Structural Parameters and Harmonic Frequencies of Minima[a] in $HO_2(X^2A'')$

method/basis[b]	energy	$-V^{c,d}$	O_aO_b	O_bH	α^e	ω_{OO}	ω_b	ω_{OH}
			Covalent					
MRCI/CVDZ	−0.6414551	53.721	1.3478	0.9771	103.26	1100.2	1425.7	3671.2
MRCI/CVTZ	−0.8240422	60.806	1.3390	0.9682	103.32	1170.0	1444.4	3727.7
CASDC/CVTZ		60.750	1.340_9^f					
CASDC/CVQZ		62.842	1.334_8^f					
CASDC/CV5Z		63.735	1.333_7^f					
CBS/CASDC/CVXZ		64.5 ± 0.3[g]	1.331_1^{fg}					
XXZLG[h]		62.69	1.334	0.972	104.12			
DMBE IV[i]		65.181	1.330	0.971	104.29			
exptl		65.1 ± 0.6[j]	1.331[k]	0.971[j]	104.3[j]			
		64.3 ± 0.8[l]						
			vdW					
MRCI/AVTZ[m]		2.07	3.14	0.974	0	220	220	3722
MRCI/CVDZ	−0.5554600	2.850	3.2179	0.9787	0	124.0	244.2	3712.9
MRCI/CVTZ	−0.7254097	2.000	3.236_7^f	0.9691	0			
CASDC/CVQZ		1.828	3.243_0^f		0			
CASDC/CV5Z		1.769	3.241_6^f		0			
CBS/CASDC/CVXZ		1.755 ± 0.007[fg]	3.240_5^{fg}		0			
MRCI/AVTZ	−0.6507968	2.691	3.1409	0.9679	0	133.8	317.6	3763.5
MRCI/AVQZ	−0.7189383	1.994	3.1730	0.9680	0	114.5	208.1	3758.2
CBS/MRCI/AVXZ[n]		1.947						
XXZLG[i]		1.800	3.168	0.971	0			
DMBE IV[i]		2.239	2.997	0.975	0	156.6	237.8	3694.9

[a]Energies in the second column are in E_h (total energy, including the Davison correction where applicable, once added 150 E_h), distances in Å, angles in deg, and frequencies (OO stretching, bending, and OH stretching or intermolecular, bending, and OH stretching as appropriate) in cm^{-1}. Unless explicitly indicated, all values in this and following table are from this work. [b]X stands for the cardinal number. [c]Dissociation energy, in kcal mol^{-1}, with Davidson's correction for MRCI and CASDC. [d]With experimental ZPE correction for covalent minimum. [e]$\alpha = \angle HO_bO_a$. [f]Obtained through a parabolic fit to data for $1.32 \le R_{O_aO_b}/Å \le 1.38$ or $3.15 \le R_{O_aO_b}/Å \le 3.30$ as appropriate: last digit uncertain. See also text. [g]From CBS(T,Q) and CBS(Q,5). [h]Calculated with MRCI/AVQZ.[57] [i]Pastrana et al.[30] (vdW minimum, this work). [j]Howard.[104] [k]Lubic et al.[106] [l]Litorja et al.[105] [m]Harding et al.[35] [n]From CBS(Q,5): see text.

dx.doi.org/10.1021/jp401384d | J. Phys. Chem. A 2013, 117, 7393−7407

Table 2. Structural Parameters and Harmonic Frequencies of Saddle Point Connecting the vdW and Deep Covalent-Type Minima[a] in $HO_2(X^2A'')$

method/basis[b]	energy	$-V^c$	O_aO_b	O_bH	α^d	ω_{inter}	ω_b	ω_{OH}
CASSCF/CVDZ[e]	−0.2023799	1.074	2.9522	0.9812	57.43	182.2	129.8*i*	3626.7
CASSCF/CVTZ	−0.2420310	0.675	3.0484	0.9738	58.65	128.1	111.1*i*	3655.3
MRCI/CVDZ[e]	−0.5538483	1.834	2.8614	0.9775	52.20	211.7	176.3*i*	3720.6
MRCI/CVTZ	−0.7243782	1.348	2.9268	0.9682	49.49			
CASDC/CVQZ		1.006	3.001_2[f]					
CASDC/CV5Z		1.029	3.036_7[f]					
CBS/CASDC/CVXZ		1.010 ± 0.007[g]	3.042_8[f]					
MRCI/AVTZ[h]		1.46	2.90	0.974	45.6	189	187*i*	3626.7
MRCI/AVTZ	−0.6492519	1.721	2.8605	0.9678	45.73	186.5	205.4*i*	3769.8
MRCI/AVQZ	−0.7180801	1.456	2.9143	0.9668	46.19	170.3	171.5*i*	3777.0
DMBE IV[i]		1.641	2.6897	0.9632	40.24	224.6	249.4*i*	3999.9

[a]Units as in Table 1. [b]Where relevant, the extrapolation is CBS(Q,5). [c]Interaction energy, in kcal mol^{-1} (with Davidson's correction for MRCI). [d]$\alpha = \angle HO_bO_a$. [e]Converged up to 1 μ E_h Å^{-1}. [f]From parabolic fit for $2.9 \leq R_{O_aO_b}/Å \leq 3.15$: last digit uncertain (possibly two last, but given for reproducibility). [g]From CBS(T,Q) and CBS(Q,5). [h]From Harding et al.[35] [i]DMBE IV PES[30] (this work).

explained from the fact that the latter included the Davidson correction. Note also that the attributes of the vdW stationary points have been determined only up to CBS(Q,5) because the highly expensive CBS(5,6) is hardly expected to influence the final result. To be emphasized is the fingerprint due to the change in nature of the intermolecular forces. Although manifesting as a small barrier in the ORC and IRC 1D plots, it is the result of a subtle change in topography of the PES, which can only find additional intricacies for larger polyatomic reactions.[12]

The energetics and structural parameters of the vdW region of configuration space are collected in Table 1 for the vdW minimum and Table 2 for the associated saddle point. As seen, there is generally a good agreement with the data from the XXZLG[56] PES. As might normally be expected, the role of polarization functions is not a negligible one. In fact, the attributes of the saddle point and vdW minimum reported in Table 2 at the MRCI/AVQZ level of theory are likely to be the most accurate reported to date. As seen, the location of the saddle point and vdW minimum tends to occur at a distance shorter by ∼0.1 Å than with CASDC whereas the energy tends to be lower by a fraction of a kcal mol^{-1}. Nevertheless, the attributes of the saddle point and minima predicted at the MRCI level of theory show significant differences, partly due to the BSSE that may be substantial for the smaller AVTZ basis. Overall, the CASDC results (particularly the CBS ones, which have been estimated from the (T,Q) and (Q,5) cardinal pairs at the optimized MRCI/AVQZ geometry) show fairly good agreement with the MRCI estimates, particularly the AVQZ one, given their extreme cost. There is also fair agreement with the ab initio calculations reported by Harding et al.[35] based on a five orbital-seven electron CASSCF reference wave function. Particularly interesting from Table 2 is the fact that the vdW minimum tends to weaken with basis set size at all levels of theory but is still far from being negligible at the CBS limit. In fact, the CBS/CASDC classical barrier height that separates this minimum from the covalent one is 0.745 ± 0.014 kcal mol^{-1}, thence larger by ∼0.2 kcal mol^{-1} than the MRCI/AVQZ estimate. It should be emphasized that the error bar in the vdW attributes qualifies the CBS extrapolation but not the error in the CASDC scheme. In this regard, one may wonder about extrapolating the MRCI results themselves. To answer this question, we have performed single-point MRCI + Q/AV5Z calculations at the optimized MRCI/AVQZ vdW minimum and at the asymptote, yielding a best value of 1.947 kcal mol^{-1}. From this and CASDC results, one gets the embracing estimate of 1.85 ± 0.1 kcal mol^{-1}. Because this simple procedure may yield meaningless results at the saddle point due to it being an avoided intersection,[109] it will not be attempted.

To pursue the discussion at a more realistic level, one requires the zero-point energy (ZPE) correction of the O···HO molecule at the vdW minimum (reactants) and at the saddle point (TS), in principle with both values calculated at the CBS limit. Unfortunately, the best force calculations here completed have been done only at the harmonic level, but this should not preclude the following discussion. The barrier height for isomerization should then be corrected by adding the difference of ZPE of the TS and vdW minimum, $\Delta E^D_{ZPE} = -0.563$ kcal mol^{-1}, yielding a corrected value of ≃0.18 kcal mol^{-1} at the MRCI/CVDZ level, enough for the vdW well to support at least one bound state. However, if the ZPE corrections that are calculated at the CASSCF/CVTZ level of theory are used to approximate a MRCI/CVTZ estimate, this implies a further decrease by 0.052 kcal mol^{-1} (difference of the ΔE^X_{ZPE} values at the CASSCF/CVTZ and D levels of theory) and hence a reduction in stability to ≃0.13 kcal mol^{-1}. On the other hand, if the extremely demanding and accurate energies and ZPE values obtained at the MRCI/AVQZ level of theory are utilized, the ZPE correction is $\Delta E^{AVQZ}_{ZPE} = -0.488$ kcal mol^{-1}, with a further lowering of stability to ≃0.05 kcal mol^{-1}. Anyhow, if vibrational states are supported by such a vdW well, they would be stable with respect to dissociation, but the barrier height to enter the deep covalent one is not sufficiently tall to allow both wells to be considered as independent. As a result, the wave functions associated with each well would be expected to mix and hence produce new wave functions. Some kind of doubling would then be observed on the calculated levels. Of course, any rigorous prediction will require full quantum dynamics calculations on an accurate global PES. Whether such states can be observed is an issue that, to our knowledge, has not yet been addressed for the title system. A further remark to note is that one expects the vdW well to enhance also the appearance of reactive resonances, a topic much studied by several groups on other PESs.[36−43,66]

3.1.3. Long-Range Interaction. We now turn to the O−OH long-range interaction potential whose components have been discussed in the literature.[110,111] It assumes the form $V = C_4R^{-4} + C_5R^{-5} + C_6R^{-6} + ...$, where only the first two leading terms of

dx.doi.org/10.1021/jp401384d | J. Phys. Chem. A 2013, 117, 7393−7407

the electrostatic series expansion plus the leading of the (induction plus) dispersion are explicit; V denotes the energy relative to the asymptote. Thus, the first two terms refer to the electrostatic interaction between the permanent quadrupole moment of atomic oxygen (Q_O) and the permanent dipole (μ_{OH}) and quadrupole (Q_{OH}) moments of OH. Explicitly, the coefficients assume the classical form:[112]

$$C_4 = \frac{3}{4} Q_O \mu_{OH} [\cos\theta(3\cos^2\theta_O - 1) - 2\sin\theta \sin\theta_O \cos\theta_O \cos(\Delta\phi)] \quad (2)$$

$$C_5 = \frac{3 Q_O Q_{OH}}{16} \times [1 - 5(\cos^2\theta + \cos^2\theta_O + 3\cos^2\theta\cos^2\theta_O) + 2(\sin\theta\sin\theta_O\cos\Delta\phi - 4\cos\theta\cos\theta_O)^2] \quad (3)$$

where $R = |\vec{R}|$ is the distance connecting O to the center-of-mass of OH and (θ, ϕ) and (θ_O, ϕ_O) are the spherical polar angles of the molecule and atom ($\Delta\phi = \phi - \phi_O$). In turn, the term R^{-6} accounts effectively for the leading dispersion (plus induction) contributions. The above coefficients can in principle be obtained with the methods of quantum chemistry but, to our knowledge, no accurate estimates were reported. Specifically, C_6 may be approximated semiempirically using the polarizabilities or related properties of the interacting species: a value of $C_6 = -23.2$ E_h a_0^6 has been estimated[113] by adding an induction contribution to a dispersion term calculated using the Slater–Kirkwood[114] method. We may then aim at knowing whether the supermolecular approach here utilized can yield a curve that decays in the long-range region as predicted above.

The problem of extracting the long-range coefficients from a fit to supermolecular calculations is an intricate one.[100,101,115] For simplicity, we begin by assuming that the above truncated expansion is sufficient to mimic the calculated data. Additionally, R is identified (without significant error) with the O_aO_b distance. If $x = R^{-1}$, the result is $x^{-4}V = C_4 + C_5x + C_6x^2$, with the coefficients being determined from a fit (I) to the data. All points between 4.7 and 20 Å were included, a range of bond distances large enough for assuming negligible charge-overlap effects (i.e., to exempt the use of damping functions[71,116]) but still far from the asymptote to avoid truncation errors. Recall that the terms of a simple polynomial form are nonorthogonal, and hence some ambiguity is unavoidable. Using atomic units and weighting democratically all points, the result from this fit I is $C_4 = -1.87 \pm 0.06$ E_h a_0^5, $C_5 = -3.01 \pm 1.42$ E_h a_0^5, and $C_6 = -133 \pm 10$ E_h a_0^6 where, for convenience, two decimal figures are kept in C_5. Figure 6 (and Figure 7) show that the fit is good. To our knowledge, the only data available for comparison is that of Clary and Werner,[113] $C_4 = -1.58$ E_h a_0^4 and $C_5 = -3.29$ E_h a_0^5, in addition to the value of C_6 given above. C_4 has been calculated from the permanent electric quadrupole moment of $O(^3P)$ and dipole moment of $OH(^2\Pi)$ ($\mu_{OH} = -1.60$ E_h a_0 and $Q_O = 0.656$ e a_0, respectively[117,118]) whereas C_5 employed instead the quadrupole moment of OH ($Q_{OH} = -1.37$ E_h a_0^2).

In calculating C_4 and C_5, Clary and Werner[113] assumed $\theta_O = 0$. With the quadrupole axis of the O atom lying always along $\vec{R}$, there is a change of sign of the potential as the angle of approach of the O atom changes from head on with the O end of OH to head on with the H end of OH. An adiabatic description is to let the electronic distribution on the O atom instantaneously adjust to the OH electronic charge distribution,

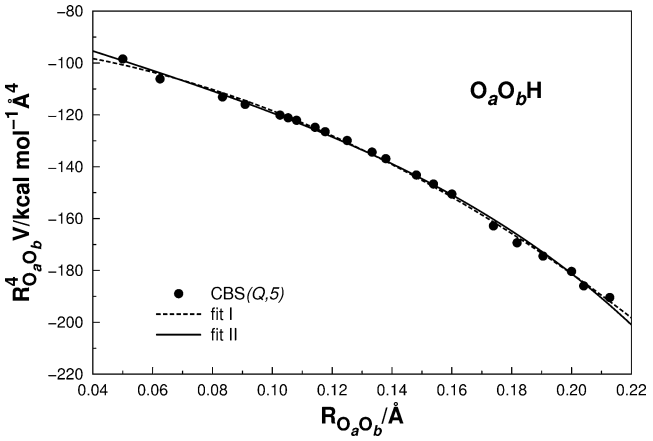

Figure 6. Fit used to approximate the C_4, C_5, and effective C_6 long-range coefficients. See the text.

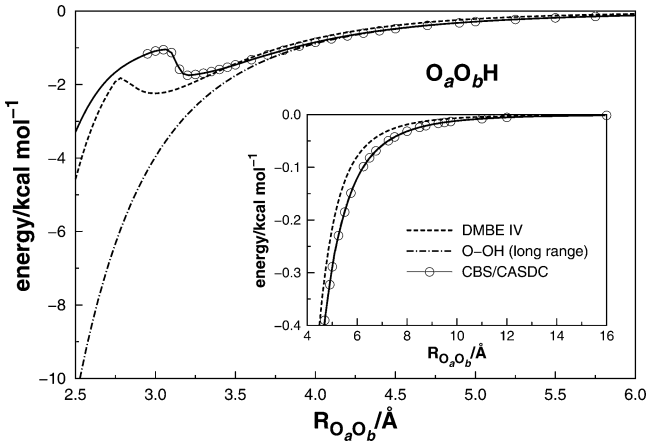

Figure 7. Comparison of the ORC path at the CBS/CASDC level of theory from the present work with the one for DMBE IV,[30] and corresponding long-range fit from the present work; reference energy as in Figure 1. See Figure 5 of the XXZLG PES paper[57] for further comparisons.

whatever the value of θ.[29] If a sine-weighted-θ averaging is then performed, the result is $\langle C_4\rangle = -0.93$ E_h a_0^4 and $\langle C_5\rangle = -1.79$ E_h a_0^5. As seen, the present estimates agree best with the Clary–Werner[113] values, because the fit refers to the minimum energy path. It also finds support on the calculated permanent electric moments of $O(^3P)$ and $OH(^2\Pi)$. Because the dipole moment is a vector and the quadrupole moment a tensor, they are best characterized by their magnitude, which in spherical coordinates assumes the form[119] $\hat{Q}_l^2 = (4\pi/2l + 1)\Sigma_m|Q_{lm}|^2$, with ($l = 1$; $m = 0, 1$). Our MRCI/CV5Z calculations yield values for these that essentially indistinguishable from the ones reported above.

As one might expect, the C_6 obtained from fit I overestimates the true value. In fact, if approximated from the isoelectronic O–F interaction through the popular geometrical mean rule using the coefficients for the homonuclear interactions,[120,121] its predicted unsigned value is $C_6 \sim 12$–15 E_h a_0^6. The above gross overestimation is then likely due to accounting in an effective way for higher-order dispersion coefficients as well as induction ones. Indeed, fit I matches the calculated curve but any assignment of the dispersion coefficients remains elusive.

In an attempt to get a realistic estimate of C_6, we followed recent work[100,101] and carried a fit (II) to a sum of damped

dx.doi.org/10.1021/jp401384d | J. Phys. Chem. A 2013, 117, 7393–7407

electrostatic, $V_{ele}(R_{O_aO_b}) = C_4\chi_4(R_{O_aO_b}) + C_5\chi_5(R_{O_aO_b})$, plus dispersion, $V_{disp}(R_{O_aO_b}) = -\sum_{n=6,8,10} C_n\chi_n(R_{O_aO_b})R_{O_aO_b}^{-n}$, terms; $\chi_n(R_{O_aO_b}/\rho)$ are charge-overlap damping functions[71,116] embedding a scaling parameter (ρ) to mimic the charge-overlap onset, and $C_{n\geq 6}$ are effective dispersion coefficients. In so doing, C_4, C_5, C_6, and ρ = 5.9 Å were treated as the only adjustable parameters, whereas C_8 and C_{10} were related to C_6 as recommended elsewhere.[100,101] As Figure 7 shows, fit II is also satisfactory over the entire range, yielding $C_4 = -1.65 \pm 0.04$ E_h a_0^4, $C_5 = (-13.4 \pm 0.8)$ E_h a_0^5, and $C_6 = 13.6 \pm 1.1$ E_h a_0^6. Although C_4 agrees well with our estimate above, and so does C_6 with our own most recent result of $C_6 = 14.1$ E_h a_0^6 from a fit to the spherically averaged component of a novel global MRCI + Q/AVQZ form for HO_2,[122] the price paid has been a poor agreement for C_5. Because this coefficient bears a large uncertainty, further estimates may be required before a definite evaluation.

3.2. Disulfanyl Radical. CASSCF and MRCI calculations have been carried out for the disulfanyl radical for values of the reaction coordinate (S_aS_b) between 1.8 and 100 Å. First the stationary points have been characterized and their attributes tightly converged, some apparently for the first time. Then, the ORC path has been calculated both inward and outward starting from the saddle point.

Figure 8 shows the optimal CASSCF and CASDC ORC paths for the reaction $HS_2 \rightleftharpoons S + SH$ as obtained with the V(X

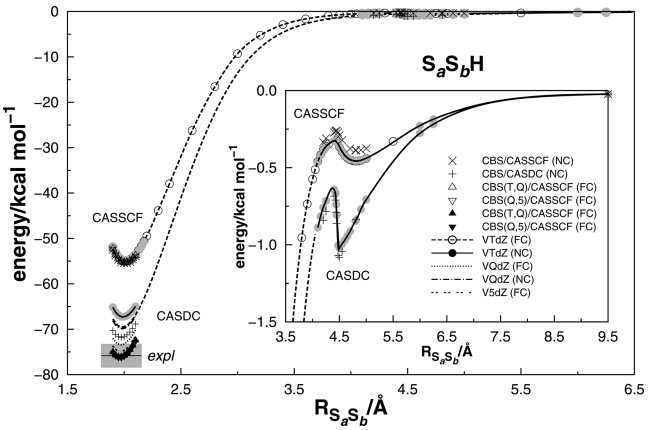

Figure 8. Optimized CASSCF, CASDC, CBS/CASSCF, and CBS/CASDC reaction paths in $HS_2 \rightleftharpoons S + SH$. For clarity, the quadruple-ζ calculations are not shown in the inset. The shaded area defines the uncertainty reported[81] for the experimental data whose averaged value is indicated by the small line segment between 1.8 and 2.15 Å. Note that the CASSCF energy at the region of the covalent minimum is well converged at the V(T+d)Z level, with all calculations giving similar results. See text.

+d)Z basis, X = T, Q, 5. First, the entire ORC path has been optimized at the CASSCF level of theory within the FC assumption, with key portions of the curve being then calculated with no closed orbitals. Naturally, the raw values of the total energy are different at the two levels of CASSCF theory, but the calculated interaction energies relative to the asymptote turn out to be very similar to each other, as can be seen from the corresponding attributes gathered in Tables 3 and 4; some values have been excluded for brevity. In an obvious notation, the corresponding correlated results will be labeled as CASDC (FC) and CASDC (NC). As for the congener HO_2 radical, the CASSCF vdW minimum does not coincide with the one at MRCI + Q level of theory but both are predicted to be collinear-like. In the present case too, the region of the ORC path between the saddle point and the vdW minimum is the one where visible differences are expected between the CASDC and the (unaffordable) directly optimized MRCI + Q results. Although reasonably sharp extrema are apparent as in the HO_2 case, there are no discontinuities at the CASDC level of theory. This can ultimately be ascribed to the floppiness of HS_2, and more directly to reasons akin to the ones pointed out for HO_2. Note that CBS extrapolated results of the covalent minimum are reported at both the FC and NC levels of theory but only at the NC level for the vdW minimum. However, as shown from the directly optimized data at the V(T +d)Z basis level, the attributes at both the FC and NC levels of theory show good agreement with each other.

The energetic and structural characterizations of the covalent and vdW minima are given in Table 3, whereas Table 4 gathers the attributes of the saddle point that connects them. Given the rather tight convergence used for locating them, all quoted figures should be significant, being given for benchmarking purposes. Two major observations stem from Table 3. First, the ORC of the disulfanyl radical calculated at the CASSCF level of theory within the FC approximation shows generally good agreement with the rather more expensive NC one. However, the CBS/CASDC curve based on the CASSCF (NC) reference wave function predicts a well depth for the covalent minimum that underestimates by 2 kcal mol^{-1} or so the CASSCF (FC) estimate. Indeed, extra FC calculations at the CASDC/V(X +d)Z (X = 5, 6) level of theory yield (upon averaging of the three CBS predictions based on a quartic fit to the calculated values for $1.900 \leq R_{OO}/\text{Å} \leq 2.050$, but still mimicking the data up to the last calculated point at 2.1 Å) a fairly conservative prediction of 76.3 ± 0.2 kcal mol^{-1} at 1.9616 ± 0.0008 Å and 76.3 ± 0.1 kcal mol^{-1} at 1.9609 ± 0.0002 Å, if only CBS(Q,5) and CBS(5,6) values are utilized.

Table 3 compares our results with the ones reported from single-reference CCSD(T) calculations by Francisco[80] and Peterson et al.,[81] both of which have also been CBS extrapolated. Francisco[80] employed the AVXZ basis set, and Peterson et al.[81] used AV(X+d)Z. These authors have further considered various corrections within the assumption of additivity. Having done the bulk of the calculations within the FC approximation, Peterson et al.[81] have in particular considered the correction due to correlating both the S 2s and 2p electrons. Moreover, a correction for relativistic effects has been added.[81] Remarkably, the agreement of our FC results with the CBS/CCSD(T) estimates of Peterson et al.[81] is within $\lesssim$0.2 kcal mol^{-1} whereas for the geometry of the minimum it is down to $\simeq$0.001 Å. In turn, the more expensive CBS result from the present work predicts a well depth of 71.9 kcal mol^{-1} at a somewhat longer bond length of 1.974 Å. Perusal of Table 3 would misleadingly suggest that the CBS/CASDC (NC) estimate questions previous values by at least 2 kcal mol^{-1}, including our own MRCI/AVXZ calculations (also FC-type), which have been utilized[70] to calibrate the global HS_2 DMBE PES. As shown later, such a difference will be attributed to the choice of basis sets utilized for the MRCI calculations. At this stage, one could think of correcting a posteriori for the S 2s and 2p correlation based on some assumption of additivity. However, this appears questionable, particularly at the multireference level of theory, and hence it has not been done. Similarly, the inclusion of relativistic effects is out of the

dx.doi.org/10.1021/jp401384d | J. Phys. Chem. A 2013, 117, 7393−7407

Table 3. Structural Parameters and Harmonic Frequencies of of Minima[a] in $HS_2(X^2A'')$

method/basis[b]	energy	$-V^{c,d}$	S_aS_b	S_bH	α^e	ω_{SS}	ω_b	ω_{SH}
			Covalent					
CBS/CCSD(T)/CBS[f]		75.90	1.9632	1.3494	101.50			
CBS+CV/CCSD(T)[f]		76.07	1.9591	1.3478	101.51			
CBS+CV+T/CCSD(T)[f]		76.04	1.9608	1.3482	101.52			
CBS/CCSD(T)[g]		74.1						
DMBE/CBS[h]		75.13	1.9636	1.3462	101.96	588	873	2597
CBS(T,Q)/CASSCF[i]		55.31	2.0084					
CBS(T,Q)/CASSCF[j]		55.45	2.0089					
CBS(Q,5)/CASSCF[i]		55.10	2.0086					
CBS(T,Q)/CASDC[i]		76.16	1.9602					
CBS(T,Q)/CASDC[j]		71.78	1.9739					
CBS(Q,5)/CASDC[i]		76.34	1.9607					
			vdW					
CASSCF/T[k]	−0.6199442	0.4573	4.8072	1.3544	0	30.3	72.0	2592.0
CASSCF/T[m)]	−0.6205988	0.452	4.8091	1.3541	0	29.2	69.0	2595.9
MRCI/T[k]	−0.9428560	0.968	4.4210	1.3434	0	43.4	129.0	2674.8
MRCI/T[l]	−1.1015249	1.093	4.4150	1.3396	0	44.1	130.7	2634.2
MRCI/Q[k]	−0.9711905	1.086	4.3524	1.3427	0	49.1	125.3	2682.3
CASDC/T[j]		1.059	4.515					
CASDC/Q[j]		1.077	4.514					
CBS(T,Q)/CASDC[j]		1.122	4.513					
MRCI/AV(T+d)Z[k]	−0.9498793	1.902	4.3047	1.3443	0	53.7	128.2	2671.2

[a]Units as in Table 1, with total energy (including the Davison correction where applicable) added 795 E_h. [b]Where only the cardinal number is given, the basis is V(X+d)Z. [c]With Davidson's correction for CASDC. [d]Classical dissociation energy, in kcal mol^{-1}. Estimated error for CASDC (NC) results is ≃0.03 kcal mol^{-1}; see text. [e]$\alpha = \angle HS_bS_a$. [f]With AV(X+d)Z basis; CBS extrapolation from CCCSD(T)/AV(X+d) (X = Q, 5) correlation energies. CBS + CV includes contributions of correlating the S 2s and 2p electrons at the CCSD(T)/cc-pwCVTZ level of theory. CBS + CV + T includes CCSDT-CCSD(T) correction for core−valence correlation with the AV(D+d)Z basis, and +T/TZ refers to contribution from CCSDT/AV(T+d)Z to CCSDT/AV(D+d)Z, and +Q to CCSDTQ/AV(D+d)Z-CCSDT/AV(D+d)Z difference. [g]From CCSD(T)/AVXZ optimization; see also original paper.[80] [h]DMBE/CBS.[70] [i]By interpolation, FC. [j]By interpolation, NC. [k]Direct optimization, FC. [l]Direct optimization, NC.

Table 4. Structural Parameters and Harmonic Frequencies of Saddle Point Connecting the vdW and Deep Covalent-Type Minima[a] in $HS_2(X^2A'')$

method/basis[b]	energy	$-V^c$	S_aS_b	S_bH	α^d	ω_{SS}	ω_b	ω_{SH}
CASSCF/T[e]	−0.6197332	0.325	4.4256	1.3539	53.11	41.7	42.7*i*	2594.0
CASSCF/T[f)]	−0.6199687	0.331	4.4281	1.3539	52.96	46.0	39.4*i*	2595.9
CASSCF/T[g]		0.326	4.422					
CASSCF/Q[h]	−0.6259352	0.280	4.4506	1.3526	54.14	36.8	40.3*i*	2602.5
CASSCF/Q[g]		0.279	4.423					
CBS(T,Q)/CASSCF[g]		0.265	4.442					
CASSCF/T[i]	−0.6203934	0.323	4.4347	1.3536	53.06	41.5	41.5*i*	2597.6
MRCI/T[e]	−0.9425986	0.807	4.2055	1.3420	36.33	59.8	83.1*i*	2681.9
MRCI/T[f]	−1.1012458	0.918	4.1747	1.3385	36.99	69.1	80.7*i*	2643.1
MRCI/Q[h]	−0.9709610	0.942	4.1497	1.3414	32.99	68.9	90.1*i*	2689.9
CASDC/T[g]		0.628	4.358					
CASDC/Q[g]		0.637	4.411					
CBS(T,Q)/CASDC[g]		0.673	4.363					
MRCI/AVTZ[i]	−0.9496043	1.729	4.1002	1.3428	32.74	74.9	103.7*i*	2679.8
MRCI/AVQZ[i]	−0.9731875	1.818	4.1207	1.3417	31.75	76.7	93.0*i*	2687.3

[a]Units as in Table 3, with energies given only for directly optimized CASSCF and MRCI values. [b]*X* stands for the cardinal number or CBS. [c]Interaction energy, in kcal mol^{-1}, with Davidson's correction for MRCI. [d]$\alpha = \angle HS_bS_a$. [e]Direct optimization, FC, with asymptote at MRCI+Q level of theory lying at −795.9413131 E_h. [f]Direct optimization, NC. [g]By interpolation, with NC approximation for CASSCF. [h]As in *e*, with MRCI+Q asymptote at −795.9694605 E_h. [i]Direct optimization, FC.

question at the MRCI level of theory, although CCSD(T) calculations[81] suggest them to be of the order of magnitude of the above-mentioned convergence error. As for the lack of size-extensitivity of the MRCI method, one may argue that use of Davidson's correction should in principle mitigate such a difficiency.[12]

Given the higher level of approximation, one might be led prima facie to conclude that the FC approximation yields acceptable CASSCF results but unreasonable MRCI ones. Such a view is difficult to sustain given the excellent agreement with the experimental data. Instead, one can argue that the V(X+d)Z basis has been developed to account for only valence correlation effects within the FC approximation, a finding

dx.doi.org/10.1021/jp401384d | J. Phys. Chem. A 2013, 117, 7393−7407

also supported from the CBS scheme, which is found to perform rather more satisfactorily within the FC scheme. Although more flexible basis sets[123,124] for core−valence correlating are available, their use was not deemed justified because 4 inner orbitals were frozen and 6 kept closed in the MRCI. Thus, the present results alert for the fact that CBS extrapolations should employ basis sets developed for the targeted calculations.

A piece of information required to further dwell at the energetics level is the ZPE correction. We will employ the ZPE correction (difference between the ZPEs of the triatomic and diatomic) obtained from the best CBS/CCSD(T) calculations:[81] $\Delta E_{ZPE} \simeq 2.04$ kcal mol^{-1}. If this is utilized jointly with the dissociation energy reported[81] from available $\Delta H_f(0\ K)$ data, one obtains for the classical dissociation energy a value of $D = 75.8 \pm 2.5$ kcal mol^{-1}. As Table 3 and Figure 8 show, the agreement of the CBS/CASDC prediction within the FC approximation with the experimental value is excellent. The geometric parameters deserve also a comment. For the covalent well, the optimum FC geometry of 1.9609 ± 0.0002 Å overlaps the estimated error bar of the experimental value[81,82] 1.9603 ± 0.0010 Å whereas, as expected from the above discussion, the NC result (1.9739 Å) exceeds the average value by ≃0.01 Å. However, the FC and NC CASDC/V(T+d)Z estimates for the latter lie relatively close to each other and remain so at the CBS/CASSCF level of theory. Although the largest geometry here obtained compares well with some of the CCSD(T) predictions in Table 3 and a reported[82] DFT estimate, it appears safe to conclude that the FC values stem from a more consistent analysis. As intuition might suggest, valence basis sets cannot be used when core electrons are correlated (especially for second row elements).

We now turn to the fingerprint left when passing from the covalent- to hydrogen-bonding (vdW) regimes. Strictly speaking a saddle point on the lowest adiabatic PES, such a feature emerges as a "scar" along the ORC path and arises (as in $HO_2 \rightleftharpoons O + OH$ and[12,107] $HO_3 \rightleftharpoons O_2 + OH$) from an avoided intersection due to the mixing of configurations pertaining to the two bonding regimes that are involved. Further toward dissociation, there is a vdW minimum that is fairly insensitive to basis set improvement. Direct optimizations at FC MRCI/V(T+d)Z and V(Q+d)Z levels of theory yielded well-depth predictions close to the corresponding NC CASDC values but, as expected, slightly deeper and slightly shifted inward for the former. If the difference of 0.009 kcal mol^{-1} relative to CASDC at the V(Q+d)Z level can be assumed to be valid at the CBS limit, the FC extrapolated well depth is predicted to be ∼1.13 kcal mol^{-1}. In turn, the CBS extrapolated classical barrier height that separates the vdW minimum from the deep covalent one is ≲0.4 kcal mol^{-1}, thence about a half of the corresponding HO_2 value. In fact, it reduces to 0.144 kcal mol^{-1} if FC directly optimized values at MRCI + Q/V(Q+d)Z level of theory are used. Being small, one wonders whether a higher-level CBS extrapolation would make it disappear. MRCI + Q/V(Q+d)Z calculations at the directly optimized V(Q+d)Z geometries have confirmed its existence, with the CBS(T,Q)/MRCI + Q classical barrier height being 0.134 kcal mol^{-1}.

Force calculations for S···HS were also done with the V(Q+d)Z basis [V(T+d)Z values are given in parentheses] but only at the harmonic level. Note that one of the positive frequencies of the vdW minimum is rather weak. For the minimum, the ZPE is of 4.193 (4.192) kcal mol^{-1} whereas for the saddle point it is of 3.944 (3.919) kcal mol^{-1}, thus yielding a ZPE-corrected barrier height of −0.115 (−0.139) kcal mol^{-1}, i.e., no barrier at all. Note further the difference between the CASDC and MRCI + Q values in Table 4, which is largely due to having not constrained the ORC path to include the true saddle point as done for the IRC path. Although given up to a few significant decimal places, the uncertainty in the values themselves relative to the true ones is then expected to be somewhat larger than suggested by the tabulated data. Unfortunately, such topographical subtleties do not appear in the global DMBE PES[70] (or any available thus far). We have also confirmed them via a tight (down to 10^{-6} E_h Å^{-1}) direct optimization at MRCI/AV(T+d)Z level of theory, i.e., with a basis of the type employed to calculate DMBE. Although a single-point calculation at 100 Å led to interaction energies that are lower by ∼1 kcal mol^{-1}, the classical barrier height is 0.173 kcal mol^{-1} (−0.151 kcal mol^{-1} with ZPE correction) in good agreement with the cheaper V(X+d)Z results. Despite some lowering on the imaginary frequency, AV(Q+d)Z calculations have indeed shown that the barrier persists even at this high computationally demanding level of theory. Thus, the above findings should bear no implications on the use of the HS_2 DMBE PES for reaction dynamics but, perhaps, at ultracold regimes.

4. POTENTIAL IMPLICATIONS FOR REACTION DYNAMICS

Consider the reaction $O(^3P) + OH(X\ ^2\Pi) \rightleftharpoons HO_2^\star \rightarrow H + O_2(X\ ^3\Sigma_g^-)$, which has been the object of extensive theoretical work.[66] Independently of the way in which the dynamics has been treated, available full quantum calculations[65] on the XXZLG PES have shown some worrying results. First, they seem to underpredict the rate constant at temperatures above 150 K. Second, the predicted T dependence appears to be qualitatively consistent with a low-T extrapolation of the earlier experimental values over the range 150−300 K, but not with the most recent experiments at the lowest temperatures.[19] Despite the fact that the calculations underlying the XXZLG PES are of high sophistication and the possibility of nonadiabatic effects cannot be excluded, such conflicting evidence has been suggested[65] to be a consequence of deficiencies on the fit. Third, the dynamics results on the XXZLG PES yield a rate constant smaller than DMBE IV, which has been attributed to the O + OH channel being slightly more attractive in the latter[56] (cf. the minimum energy paths in Figure 5 of this reference).

With the above results in mind, it is relevant to note from Figure 3 that OH rotates during the transition from hydrogen- to covalent-bonding. Such a motion will create a torque that may bear implications on the dynamics, particularly at low energies.[122] In turn, a careful analysis of our results at mid-distances that encompass the vdW minimum corroborates that the CBS potential is somewhat less attractive there, in agreement with the above observation for the XXZLG PES.[56] However, it becomes the most attractive beyond 5 Å or so, where larger basis sets are expected to recover more dynamical correlation. This is best seen from Figure 7 (cf. Figure 5 of the XXZLG PES paper[57]), which shows that the CBS/CASDC PES predicts a somewhat weaker vdW minimum than DMBE IV but a similar (even slightly stronger) long-range attraction. This raises yet another concern, namely on the use of splines to fit long-range interactions (as in the XXZLG PES), an issue likely valid also for related seminumerical techniques. Indeed, an accurate description of the long-range details should pose serious difficulties to spline-fitting techniques because dense

dx.doi.org/10.1021/jp401384d | J. Phys. Chem. A 2013, 117, 7393−7407

grids become unaffordable due to the wide regions of involved configuration space. The present work also suggests that the endeavor can be too computationally intensive for attempting accurate (MRCI + Q) on-the-fly dynamics. Thus, improved methods based on analytic modeling[71,72,122,125] may offer a way out if low-energy reaction dynamics is at stake, particularly at cold and ultracold regimes. Indeed, the subtleties of the H-bonding to covalent-bonding transition urge extreme care, with this work providing, to our knowledge, the first attempt to characterize at a high level of accuracy the saddle point that delimits such regimes on the adiabatic ground-state PES of the title systems.

5. CONCLUDING REMARKS

Providing a generalization of the popular HFD model for closed-shell interactions, the CASDC scheme has been shown to be a simple tool for exploring reaction paths. If basic features is all that is required, the ORC path may suffice per se. If accurate energetic and geometric attributes are envisaged, the CASDC scheme based on the IRC path is recommended. Applied thus far to HY_2 and HY_3 (Y = O, S) radicals, we envisage no reason for it not being reliable with other systems too. Indeed, conversely to many existing composite schemes, CASDC is physically sound in that it uses the two complementary (CASSCF and dc) parts of the total energy, thus relying only on the fact that the pointwise calculations of the total energy along the optimum CASSCF reaction path will capture the required dc. Untested in the present ORC scheme are reactions where two or more bonds are simultaneously broken or formed. Although a possible generalization could be to treat two or more coordinates as inactive (i.e., define a 2D or larger-dimensionality reaction surface), it may turn out to be simpler to consider the IRC path itself or even a hybrid based partly on IRC and ORC. Of course, the former requires prior knowledge of the saddle point location, often a laborious task, with the ORC path providing a good starting guess. If no optimization is done, the CASDC scheme can be used to obtain PES cuts (and hence global PESs), an approach that finds inspiration in Walch's[87] (and references therein) work. Clearly, although further testing is required, our results provide promising evidence for acceptance because CASDC is both sound and cost-effective. Regarding the numerical values of the attributes here reported, they possibly are the most reliable available for the title reactions.

AUTHOR INFORMATION

Corresponding Author

†E-mail: varandas@qtvs1.qui.uc.pt.

Notes

The authors declare no competing financial interest.

ACKNOWLEDGMENTS

This work is financed by FEDER through "Programa Operacional Factores de Competitividade - COMPETE" and national funds under the auspices of Fundação para a Ciência e a Tecnologia, Portugal (projects PTDC/QUI-QUI/099744/2008, and PTDC/AAC-AMB/099737/2008).

REFERENCES

(1) Murrell, J. N.; Laidler, K. J. Symmetries of Activated Complexes. *J. Chem. Soc., Faraday Trans.* **1968**, *64*, 371−377, DOI: 10.1039/tf9686400371.

(2) Glasstone, S.; Laidler, K.; Eyring, H. *The Theory of Rate Processes*; McGraw-Hill: New York, 1941.

(3) Brown, A.; Dewar, M. J. S.; Schoeller, W. MINDO[Modified Intermediate Neglect of differential Overlap]/2 Study of the Cope Rearrangement. *J. Am. Chem. Soc.* **1972**, *92*, 5516−5517, DOI: 10.1021/ja00721a038.

(4) Dewar, M. J. S.; Kirschner, S. MINDO [Modified Intermediate Neglect of Differential Overlap]/2 Study of Aromatic ("Allowed") Electrocyclic Reactions of Cyclopropyl and Cyclobutene. *J. Am. Chem. Soc.* **1971**, *93*, 4290−4291, DOI: 10.1021/ja00746a033.

(5) McIver, J. W.; Komornicki, A. Structure of Transition States in Organic Reactions. General Theory and an Application to the Cyclobutene-Butadiene Isomerization Using a Semiempirical Molecular Orbital Method. *J. Am. Chem. Soc.* **1972**, *94*, 2625−2633, DOI: 10.1021/ja00763a011.

(6) Hayes, D. M.; Morokuma, K. Theoretical Studies of Carbonyl Photochemistry. I. Ab Initio Potential Energy Surfaces for the Photodissociation $H_2CO^* \rightarrow H + HCO$. *Chem. Phys. Lett.* **1972**, *12*, 539−543, DOI: 10.1016/0009-2614(72)80003-4.

(7) Jaffe, R. L.; Hayes, D. L.; Morokuma, K. Photodissociation of Formaldehyde: Potential Energy Surfaces for $H_2CO \rightarrow H_2 + CO$. *J. Chem. Phys.* **1974**, *60*, 5108−5109, DOI: 10.1063/1.1681029.

(8) Fukui, K. Formulation of the Reaction Coordinate. *J. Phys. Chem.* **1970**, *74*, 4161−4163, DOI: 10.1021/j100717a029.

(9) Ishida, K.; Morokuma, K.; Komornicki, A. The Intrinsic Reaction Coordinate. An Ab Initio Calculation for $HNC \rightarrow HCN$ and $H^- + CH_4 \rightarrow CH_4 + H^-$. *J. Chem. Phys.* **1977**, *66*, 2153−2156, DOI: 10.1063/1.434152.

(10) Maeda, S.; Morokuma, K. Finding Reaction Pathways of Type A + B → X: Toward Systematic Prediction of Reaction Mechanisms. *J. Chem. Theory Comput.* **2011**, *7*, 2335−2345, DOI: 10.1021/ct200290m.

(11) Helgaker, T.; Jørgensen, P.; Olsen, J. *Molecular Electronic-Structure Theory*; Wiley: Chichester, U.K., 2000.

(12) Varandas, A. J. C. Ab Initio Treatment of Bond-Breaking Reactions: Accurate Course of HO_3 Dissociation and Revisit to Isomerization. *J. Chem. Theory Comput.* **2012**, *8*, 428−441, DOI: 10.1021/ct200773b.

(13) Wayne, R. P. *Chemistry of Atmospheres*, 3rd ed.; Oxford University Press: Oxford, U.K., 2002.

(14) Smith, I. W. M.; Herbst, E.; Chang, Q. Rapid Neutral-Neutral Reactions at Low Temperatures: A New Network and First Results for TMC-1. *Mon. Not. R. Astron. Soc.* **2004**, *350*, 323−330, DOI: 10.1111/j.1365-2966.2004.07656.x.

(15) Quan, D. H.; Herbst, E.; Millar, T. J.; Hassel, G. E.; Lin, S. Y.; Guo, H.; Honvault, P.; Xie, D. Q. New Theoretical Results Concerning the Interstellar Abundance of Molecular Oxygen. *Astrophys. J.* **2008**, *681*, 1318−1326, DOI: 10.1086/588007.

(16) Sabbah, H.; Biennier, L.; Sims, I. R.; Georgievskii, Y.; Klippenstein, S. J.; Smith, I. W. M. Understanding Reactivity at Very Low Temperatures: The Reactions of Oxygen Atoms With Alkenes. *Science* **2007**, *317*, 102−105, DOI: 10.1126/science.1142373.

(17) Herbst, E.; Klemperer, W. Formation and Depletion of Molecules in Dense Interstellar Clouds. *Astrophys. J.* **1973**, *185*, 505−534, DOI: 10.1086/152436.

(18) Larsson, B.; et al. Molecular Oxygen in the ρiuchi loud. *Astrophys. J.* **2007**, *466*, 999−1003, DOI: 10.1051/0004-6361:20065500.

(19) Carty, D.; Goddard, A.; Kohler, S. P. K.; Sims, I. R.; Smith, I. W. M. Kinetics of the Radical-Radical Reaction, $O(^3P_J) + OH(X\,^2\Pi_\Omega) \rightarrow O_2 + H$, at Temperatures Down to 39 K. *J. Phys. Chem. A* **2006**, *110*, 3101−3109, DOI: 10.1021/jp054429u.

(20) Melius, C. F.; Blint, R. J. Potential-Energy surface of the HO_2 Molecular-System. *Chem. Phys. Lett.* **1979**, *64*, 183−189, DOI: 10.1016/0009-2614(79)87305-4.

(21) Lemon, W. J.; Hase, W. L. A Potential-Energy Function for the Hydroperoxyl Radical. *J. Phys. Chem.* **1987**, *91*, 1596−1602, DOI: 10.1021/j100290a061.

(22) Walch, S. P.; Rohlfing, C. M.; Melius, C. F.; Bauschlicher, C. W., Jr. Theoretical Characterization of the Minimum Energy Path for the Reaction H + O_2 → $HO_2^\star$ → HO + O. *J. Chem. Phys.* **1988**, *88*, 6273−6281, DOI: 10.1063/1.454466.
(23) Walch, S. P.; Rohlfing, C. M.; Melius, C. F.; Baushlicher, C. W. Erratum: Theoretical Characterization of the Minimum Energy Path for the Reaction H + O_2 → $HO_2^\star$ → HO + O [*J. Chem. Phys.* **1988**, *88*, 6273]. *J. Chem. Phys.* **1989**, *90*, 7613−7613, DOI: 10.1063/1.456711.
(24) Walch, S. P.; Rohlfing, C. M. Theoretical Characterization of the Minimum Energy Path for the Reaction H + O_2 → $HO_2^\star$ → HO + O. 2. The Potential for H Atom Exchange in HO_2. *J. Chem. Phys.* **1989**, *91*, 2373−2375, DOI: 10.1063/1.457047.
(25) Walch, S. P.; Duchovic, R. J. Theoretical Characterization of the Minimum Energy Path for the Reaction H + O_2 → $HO_2^\star$ → HO + O. 3. Computed Points to Define a Global Potential-Energy Surface. *J. Chem. Phys.* **1991**, *94*, 7068−7075, DOI: 10.1063/1.460240.
(26) Walch, S. P.; Duchovic, R. J. Erratum: Theoretical Characterization of the Minimum Energy Path for the Reaction H + O_2 → $HO_2^\star$ → HO + O. 3. Computed Points to Define a Global Potential-Energy Surface. [*J. Chem. Phys.* **1991**, *94*, 7068]. *J. Chem. Phys.* **1992**, *96*, 4050−4050, DOI: 10.1063/1.462903.
(27) Klimo, V.; Bittererová, M.; Biscupic, S.; Urban, J. Quasi-Classical Trajectory Study of H + O_2→OH + O at Temperatures From 500 to 2000 K. *Chem. Phys.* **1993**, *173*, 367−675, DOI: 10.1016/0301-0104(93)80152-Y.
(28) Varandas, A. J. C.; Brandão, J. A Double Many-Body Expansion of Molecular Potential Energy Functions. II. Application to Selected AB_2-Type van der Waals Molecules and more Stable Molecules: The Ground-State Surfaces of HeH_2, $HeLi_2$ and HO_2. *Mol. Phys.* **1986**, *57*, 387−414, DOI: 10.1080/00268978600100311.
(29) Varandas, A. J. C.; Brandão, J.; Quintales, A. M. A Realistic $HO_2\tilde{X}(^2A'')$ Potential Energy Surface From the Double Many-Body Expansion Method. *J. Phys. Chem.* **1988**, *92*, 3732−3742, DOI: 10.1021/j100324a010.
(30) Pastrana, M. R.; Quintales, L. A. M.; Brandão, J.; Varandas, A. J. C. Recalibration of a Single-Valued Double Many-Body Expansion Potential-Energy Surface for Ground-State HO_2 and Dynamics Calculations for the O + OH → O2 + H Reaction. *J. Phys. Chem.* **1990**, *94*, 8073−8080, DOI: 10.1021/j100384a019.
(31) Kendrick, B.; Pack, R. T. Potential-Energy Surfaces for the Low-Lying $^2A''$ and $^2A'$ States of HO_2: Use of the Diatomics in Molecules Model to fit Ab-Initio Data. *J. Chem. Phys.* **1995**, *102*, 1994−2012, DOI: 10.1063/1.468765.
(32) Osmann, G.; Bunker, P. R.; Jensen, P.; Buenker, R. J.; Gu, J. P.; Hirsch, G. A Theoretical Investigation of the Renner Interactions and Magnetic Dipole Transitions in the $\tilde{A} - \tilde{X}$ Electronic Band System of HO_2. *J. Mol. Spectrosc.* **1999**, *197*, 262−274, DOI: 10.1006/jmsp.1999.7919.
(33) Jensen, P.; Buenker, R. J.; Gu, J. P.; Osmann, G.; Bunker, P. R. Refined Potential-Energy Surfaces for the $\tilde{X}^2A''$ and $\tilde{A}^2A'$ Electronic States of the HO_2 Molecule. *Can. J. Phys.* **2001**, *79*, 641−652, DOI: 10.1139/p01-018.
(34) Harding, L. B.; Troe, J.; Ushakov, V. G. Classical Trajectory Calculations of the High Pressure Limiting Rate Constants and of Specific Rate Constants for the Reaction H + O_2→HO_2: Dynamic Isotope Effects Between Tritium + O_2 and Muonium + O_2. *Phys. Chem. Chem. Phys.* **2000**, *2*, 631−642, DOI: 10.1039/a908929b.
(35) Harding, L. B.; Maergoiz, A. I.; Troe, J.; Ushakov, V. G. Statistical Rate Theory for the HO + O ↔ HO_2 ↔ H + O_2 Reaction System: SACM/CT Calculations Between 0 and 5000 K. *J. Chem. Phys.* **2000**, *113*, 11019−11034, DOI: 10.1063/1.1314374.
(36) Zhang, D. H.; Zhang, J. Z. H. Quantum Reactive Scattering Calculations with a Deep Well: Time-Dependent calculation for H + O_2 Reaction and Bound state Characterization for HO_2. *J. Chem. Phys.* **1994**, *101*, 3671−3678, DOI: 10.1063/1.467551.
(37) Kendrick, B.; Pack, R. T. Recombination Resonances in Thermal H + O_2 Scattering. *Chem. Phys. Lett.* **1995**, *235*, 291−296, DOI: 10.1016/0009-2614(95)00116-L.
(38) Mandelshtam, V. A.; Grozdanov, T. P.; Taylor, H. S. Bound States and Resonances of the Hydroperoxyl Radical HO_2: An Accurate Quantum Mechanical Calculation Using Filter Diagonalization. *J. Chem. Phys.* **1995**, *103*, 10074−10084, DOI: 10.1063/1.469910.
(39) Dobbyn, A. J.; Stumpf, M.; Keller, H.-M.; Hase, W. L.; Shinke, R. Theoretical study of the Unimolecular Dissociation HO_2→H + O_2. I. Calculation of the Bound States of HO_2 up to the Dissociation Threshold and Their Statistical Analysis. *J. Chem. Phys.* **1995**, *103*, 9947−9962, DOI: 10.1063/1.469884.
(40) Barclay, V. J.; Hamilton, I. P. Theoretical-Study of Fermi Resonance in the Vibrational-Spectrum of HO_2. *J. Chem. Phys.* **1995**, *103*, 2834−2834, DOI: 10.1063/1.470519.
(41) Chen, R.; Guo, H. Benchmark Calculations of Bound States of HO_2 via Basic Lanczos Algorithm. *Chem. Phys. Lett.* **1997**, *277*, 191−198, DOI: 10.1016/S0009-2614(97)00907-X.
(42) Wu, X. T.; Hayes, E. F. HO_2 Rovibrational Eigenvalue Studies for Nonzero Angular Momentum. *J. Chem. Phys.* **1997**, *107*, 2705−2719, DOI: 10.1063/1.474630.
(43) Zhang, H.; Smith, S. C. Calculation of Bound and Resonance States of HO_2 for Nonzero Total Angular Momentum. *J. Chem. Phys.* **2003**, *118*, 10042−10050, DOI: 10.1063/1.1572132.
(44) Pack, R. T.; Butcher, E. A.; Parker, G. A. Accurate Quantum Probabilities and Threshold Behavior of the H + O_2 Combustion Reaction. *J. Chem. Phys.* **1993**, *99*, 9310−9313, DOI: 10.1063/1.465548.
(45) Pack, R. T.; Butcher, E. A.; Parker, G. A. Accurate Three-Dimensional Quantum Probabilities and Collision Lifetimes of the H + O_2 Combustion Reaction. *J. Chem. Phys.* **1995**, *102*, 5998−6012, DOI: 10.1063/1.469334.
(46) Kendrick, B.; Pack, R. T. Geometric Phase Effects in the Resonance Spectrum, State-to-State Transition Probabilities and Bound State Spectrum of HO_2. *J. Chem. Phys.* **1997**, *106*, 3519−3539, DOI: 10.1063/1.473449.
(47) Dai, J.; Zhang, J. Z. H. Time-Dependent Wave Packet Approach to State-to-State Reactive Scattering and Application to H + O_2 Reaction. *J. Phys. Chem.* **1996**, *100*, 6898−6903, DOI: 10.1021/jp9536662.
(48) Groenenboom, G. C. Discrete Variational Quantum Reactive Scattering Method With Optimal Distorted Waves. II. Application to the Reaction H + O_2→OH + O. *J. Chem. Phys.* **1998**, *108*, 5677−5682, DOI: 10.1063/1.475977.
(49) Meijer, A. J. H. M.; Goldfield, E. M. Time-Dependent Quantum Mechanical Calculations on H + O_2 for Total Angular Momentum J > 0. *J. Chem. Phys.* **1998**, *108*, 5404−5413, DOI: 10.1063/1.475929.
(50) Meijer, A. J. H. M.; Goldfield, E. M. Time-Dependent Quantum Mechanical Calculations on H + O_2 for Total Angular Momentum J > 0. II. On the Importance of Coriolis Coupling. *J. Chem. Phys.* **1999**, *110*, 870−880, DOI: 10.1063/1.478054.
(51) Goldfield, E. M.; Meijer, A. J. H. M. Time-Dependent Quantum Mechanical Calculations on H + O_2 for Total Angular Momentum J > 0. III. Total Cross Sections. *J. Chem. Phys.* **2000**, *113*, 11055−11062, DOI: 10.1063/1.1326904.
(52) Abu Bajeh, M.; Goldfield, E. M.; Hanf, A.; Kappel, C.; Meijer, A. J. H. M.; Volpp, H.-R.; Wolfrum, J. Dynamics of the H + O_2 → O + OH Chain-Branching Reaction: Accurate Quantum Mechanical and Experimental Absolute Reaction Cross Sections. *J. Phys. Chem. A* **2001**, *105*, 3359−3364, DOI: 10.1021/jp0036137.
(53) Zhang, H.; Smith, S. C. Chebyshev Real Wave Packet Propagation: H + $O_2(J = 0)$ State-to-State Reactive Scattering Calculations. *J. Chem. Phys.* **2002**, *117*, 5174−5182, DOI: 10.1063/1.1499123.
(54) Zhang, H.; Smith, S. C. Efficient Time-Independent Wave Packet Scattering Calculations Within a Lanczos Subspace: H + $O_2(J = 0)$ State-to-State Reaction Probabilities. *J. Chem. Phys.* **2002**, *116*, 2354−2360, DOI: 10.1063/1.1429951.
(55) Hankel, M.; Smith, S. C.; Meijer, A. J. H. M. State-to-State Reaction Probabilities for the H + $O_2(v,j)$→O + OH(v',j') Reaction on Three Potential Energy Surfaces. *J. Chem. Phys.* **2007**, *127*, 064316 DOI: 10.1063/1.2762220.

(56) Xu, C.; Xie, D.; Honvault, P.; Lin, S. Y.; Guo, H. Rate Constant for $OH(^2\Pi) + O(^3P) \rightarrow H(^2S) + O_2(^3\Sigma_g^-)$ Reaction on an Improved Ab Initio Potential Energy Surface and Implications for the Interstellar Oxygen Problem. *J. Chem. Phys.* **2007**, *127*, 024304 DOI: 10.1063/1.2753484.
(57) Xu, C.; Xie, D.; Zhang, D. H.; Lin, S. Y.; Guo, H. A New Ab Initio Potential-Energy Surface of $HO_2(X^2A'')$ and Quantum Studies of HO_2 Vibrational Spectrum and Rate Constants for the $H + O_2 \rightarrow O + OH$ Reactions. *J. Chem. Phys.* **2005**, *122*, 244305 DOI: 10.1063/1.1944290.
(58) Ma, J.; Lin, S. Y.; Guo, H.; Sun, Z.; Zhang, D. H.; Xie, D. State-to-State Quantum Dynamics of the $O(^3P) + OH(^2\Pi) \rightarrow H(^2S) + O_2(^3\Sigma_g^-)$ Reaction. *J. Chem. Phys.* **2010**, *133*, 054302 DOI: 10.1063/1.3455431.
(59) Dunning, T. H., Jr. Gaussian Basis Sets For Use in Correlated Molecular Calculations. I. The Atoms Boron Through Neon and Hydrogen. *J. Chem. Phys.* **1989**, *90*, 1007−1023, DOI: 10.1063/1.456153.
(60) Kendall, R. A.; Dunning, T. H., Jr.; Harrison, R. J. Electron Affinities of the First-Row Atoms Revisited. Systematic Basis Sets and Wave Functions. *J. Chem. Phys.* **1992**, *96*, 6796−6806, DOI: 10.1063/1.462569.
(61) Woon, D. E.; Dunning, T. H., Jr. Gaussian Basis Sets for Use in Correlated Molecular Calculations. IV. Calculation of Static Electrical Response Properties. *J. Chem. Phys.* **1994**, *100*, 2975−2988, DOI: 10.1063/1.466439.
(62) Quéméner, G.; Balakrishnan, N.; Kendrick2, B. K. Quantum Dynamics of the $O + OH \rightarrow H + O_2$ Reaction at Low Temperatures. *J. Chem. Phys.* **2008**, *129*, 224309 DOI: 10.1063/1.3035904.
(63) Lin, S. Y.; Guo, H.; Honvault, P.; Xu, C.; Xie, D. Accurate Quantum Mechanical Calculations of Differential and Integral Cross Sections and Rate Constant for the O + OH Reaction Using an Ab Initio Potential Energy Surface. *J. Chem. Phys.* **2007**, *128*, 014303 DOI: 10.1063/1.2812559.
(64) Jorfi, M.; Honvault, P.; Halvick, P.; Lin, S. Y.; Guo, H. Quasiclassical Trajectory Scattering Calculations for the $OH + O \rightarrow H + O_2$ Reaction: Cross Sections and Rate Constants. *Chem. Phys. Lett.* **2008**, *468*, 53−57, DOI: 10.1016/j.cplett.2008.07.069.
(65) Lique, F.; Jorfi, M.; Honvault, P.; Halvick, P.; Lin, S. Y.; Guo, H.; Xie, D. Q.; Dagdigian, P. J.; Klos, J.; Alexander, M. H. $O + OH \rightarrow O_2 + H$: A Key Reaction for Interstellar Chemistry. New Theoretical Results and Comparison With Experiment. *J. Chem. Phys.* **2009**, *131*, 221104 DOI: 10.1063/1.3274226.
(66) Guo, H. Quantum Dynamics of Complex-Forming Bimolecular Reactions. *Int. Rev. Phys. Chem.* **2012**, *31*, 1−68, DOI: 10.1080/0144235X.2011.649999.
(67) Varandas, A. J. C. Reactive and Non-Reactive Vibrational Quenching in O + OH Collisions. *Chem. Phys. Lett.* **2004**, *396*, 182−190, DOI: 10.1016/j.cplett.2004.08.023.
(68) Caridade, P. J. S. B.; Horta, J. Z. J.; Varandas, A. J. C. Implications of the O + OH Reaction in Hydroxyl Nightglow Modeling. *Atmos. Chem. Phys.* **2013**, *12*, 1−33, DOI: 10.5194/acp-13-1-2013.
(69) Basis sets were obtained from the Extensible Computational Chemistry Environment Basis Set Database, Version 02/25/04, as developed and distributed by the Molecular Science Computing Facility, Environmental and Molecular Sciences Laboratory, which is part of the Pacific Northwest Laboratory, P.O. Box 999, Richland, WA 99352, U.S.A., and funded by the U.S. Department of Energy. The Pacific Northwest Laboratory is a multiprogram laboratory operated by Battelle Memorial Institute for the U.S. Department of Energy under contract DE-AC06−76RLO 1830. Contact Karen Schuchardt for further information.
(70) Song, Y. Z.; Varandas, A. J. C. Accurate Double Many-Body Expansion Potential Energy Surface for Ground-State HS_2 Based on Ab Initio Data Extrapolated to the Complete Basis Set Limit. *J. Phys. Chem. A* **1999**, *115*, 5274−5283, DOI: 10.1021/jp201980m.
(71) Varandas, A. J. C. Intermolecular and Intramolecular Potentials: Topographical Aspects, Calculation, and Functional Representation via a DMBE Expansion Method. *Adv. Chem. Phys.* **1988**, *74*, 255−338, DOI: 10.1002/9780470141236.ch2.
(72) Varandas, A. J. C. In *Conical Intersections: Electronic Structure, Spectroscopy and Dynamics*; Domcke, W., Yarkony, D. R., Köppel, H., Eds.; Advanced Series in Physical Chemistry; World Scientific Publishing: Singapore, 2004; Chapter 5, pp 205−270; doi 10.1142/9789812565464_0005.
(73) Porter, G. The Absorption Spectroscopy of Substances of Short Life. *Discuss. Faraday Soc.* **1950**, *9*, 60−69, DOI: 10.1039/DF9500900060.
(74) Yamamoto, S.; Saito, S. Microwave Spectrum and Molecular Structure of the HS_2 Radical. *Can. J. Phys.* **1994**, *72*, 954−962, DOI: 10.1139/p94-125.
(75) Isoniemi, E.; Khriachtchev, L.; Pettersson, M.; Räsänen, M. Infrared Spectroscopy and 266 nm Photolysis of H_2S_2 in Solid Ar. *Chem. Phys. Lett.* **1999**, *311*, 47−54, DOI: 10.1016/S0009-2614(99)00756-3.
(76) Ashworth, S. H.; Fink, E. H. The High Resolution Fourier-Transform Chemiluminescence Spectrum of the HS_2 Radical. *Mol. Phys.* **2007**, *105*, 715−725, DOI: 10.1080/00268970601146880.
(77) Sannigrahi, A. B.; Peyerimhoff, S. D.; Buenker, R. J. Theoretical Study of the Geometry and Spectrum of the HS_2 Radical. *Chem. Phys. Lett.* **1977**, *46*, 415−421, DOI: 10.1016/0009-2614(77)80618-0.
(78) Owens, Z. T.; Larkin, J. D.; Schaefer, H. F., III. Hydrogen Bridging in the Compounds $X_2H(X$ = Al,Si,P,S). *J. Chem. Phys.* **2006**, *125*, 164322 DOI: 10.1063/1.2363375.
(79) Denis, P. A. Theoretical Characterization of the Thiosulfeno Radical, HS_2. *Chem. Phys. Lett.* **2006**, *422*, 434−438, DOI: 10.1016/j.cplett.2006.02.107.
(80) Francisco, J. S. Sulfur Atom Exchange in the Reaction of SH Radicals With S Atoms. *J. Chem. Phys.* **2007**, *126*, 214301 DOI: 10.1063/1.2735299.
(81) Peterson, K. A.; Mitrushchenkov, A.; Francisco, J. S. A Theoretical Study of the Spectroscopic Properties of the Ground and First Excited Electronic State of HS_2. *Chem. Phys.* **2008**, *346*, 34−44, DOI: 10.1016/j.chemphys.2008.02.042.
(82) Tanimoto, M.; Klaus, T.; Müller, H. S.; Winnewisser, G. Rotational Spectra of the Thiosulfeno Radical, HSS and DSS, between 0.3 and 0.9 THz. *J. Mol. Spectrosc.* **2000**, *199*, 73−80, DOI: 10.1006/jmsp.1999.7990.
(83) Hepburn, J.; Scoles, G.; Penco, R. A Simple But Reliable Method for the Prediction of Intermolecular Potentials. *Chem. Phys. Lett.* **1975**, *36*, 451−456, DOI: 10.1016/0009-2614(75)80278-8.
(84) Podeszwa, R.; Pernal, K.; Patkowski, K.; Szalewicz, K. Extension of the Hartree-Fock Plus Dispersion Method by First-Order Correlation Effects. *J. Phys. Chem. Lett.* **2010**, *1*, 550−555, DOI: 10.1021/jz9002444.
(85) Murrell, J. N.; Varandas, A. J. C. Perturbation Calculations of Rare-Gas Potentials Near the van der Waals Minimum. *Mol. Phys.* **1975**, *30*, 223−236, DOI: 10.1080/00268977500101911.
(86) Jensen, F. *Introduction to Computational Chemistry*, 2nd ed.; Wiley: Chichester, U.K., 2006.
(87) Walch, S. P. Theoretical Characterization of the Potential Energy Surface for NH + NO. *J. Chem. Phys.* **1999**, *98*, 1170−1177, DOI: 10.1063/1.464340.
(88) Dunning, T. H., Jr; Peterson, K. A.; Wilson, A. K. Gaussian Basis Sets For Use in Correlated Molecular Calculations. X. The Atoms Aluminum Through Argon Revisited. *J. Chem. Phys.* **2001**, *114*, 9244−9253, DOI: 10.1063/1.1367373.
(89) Szalay, P. G.; Müller, T.; Gidofalvi, G.; Lischka, H.; Shepard, R. Multiconfiguration Self-Consistent Field and Multireference Configuration Interaction Methods and Applications. *Chem. Rev.* **2012**, *112*, 108−181, DOI: 10.1021/cr200137a.
(90) Knowles, P. J.; Werner, H. J. An Efficient Method for the Evaluation of Coupling Coefficients in Configuration Interaction Calculations. *Chem. Phys. Lett.* **1988**, *145*, 514−522, DOI: 10.1016/0009-2614(88)87412-8.

(91) Werner, H. J.; Knowles, P. J. An Efficient Internally Contracted Multiconfiguration-Reference Configuration Interaction Method. *J. Chem. Phys.* **1988**, *89*, 5803 DOI: 10.1063/1.455556.
(92) Werner, H.-J.; et al. *MOLPRO*, Version 2010.1, a package of *ab initio* programs. See http://www.molpro.net.
(93) Times per MRCI/CVXZ point on a 64 bit double-core double-processor@1.87 GHz near the covalent minimum are (in hours): 3.0, 5.2, 27, 143 for X = D,T,Q, 5, respectively.
(94) Varandas, A. J. C. Extrapolating to the One-Electron Basis-Set Limit in Electronic Structure Calculations. *J. Chem. Phys.* **2007**, *126*, 244105 DOI: 10.1063/1.2741259.
(95) Karton, A.; Martin, J. M. L. Comment on "Estimating the Hartree-Fock Limit From Finite Basis Set Calculations". *Theor. Chem. Acc.* **2006**, *115*, 330−333, DOI: 10.1007/s00214-005-0028-6.
(96) Jensen, F. Estimating the Hartree-Fock Limit From Finite Basis Set Calculations. *Theor. Chem. Acc.* **2005**, *113*, 267−273, DOI: 10.1007/s00214-005-0635-2.
(97) Varner, M. E.; Harding, M. E.; Vázquez, J.; Gauss, J.; Stanton, J. F. Dissociation Energy of the HOOO Radical. *J. Phys. Chem. A* **2009**, *113*, 11238−11241, DOI: 10.1021/jp907262s.
(98) Boys, F.; Bernardi, F. The Calculation of Small Molecular Interactions by the Differences of Separate Total Energy. Some Procedures With Reduced Error. *Mol. Phys.* **1970**, *19*, 553−566, DOI: 10.1080/00268977000101561.
(99) Varandas, A. J. C. Can Extrapolation to the Basis Set Limit be an Alternative to the Counterpoise Correction? A Study on the Helium Dimer. *Theor. Chem. Acc.* **2008**, *119*, 511−521, DOI: 10.1007/s00214-008-0419-6.
(100) Varandas, A. J. C. Extrapolation to the Complete Basis Set Limit Without Counterpoise. The Pair Potential of Helium Revisited. *J. Phys. Chem. A* **2010**, *114*, 8505−8516, DOI: 10.1021/jp908835v.
(101) Varandas, A. J. C. Correction to "Extrapolation to the Complete Basis Set Limit without Counterpoise. The Pair Potential of Helium Revisited" [*J. Phys. Chem. A* **2010**, *114*, 8505]. *J. Phys. Chem. A* **2011**, *115*, 2668−2668, DOI: 10.1021/jp201221f.
(102) Burkholder, J. B.; Hammer, P. D.; Howard, C. J.; Towle, J. P.; Brown, J. M. Fourier Transform Spectroscopy of the ν_2 and ν_3 Bands of HO_2. *J. Mol. Spectrosc.* **1992**, *151*, 493−512, DOI: 10.1016/0022-2852(92)90582-9.
(103) Summers, M. E.; Conway, R. R.; Siskind, D. E.; Stevens, M. H.; Offermann, D.; Riese, M.; Preusse, P.; Strobel, D. F.; Russell, J. M., III. Implications of Satellite OH Observations for Middle Atmospheric H_2O and Ozone. *Science* **1997**, *277*, 1967−1970, DOI: 10.1126/science.277.5334.1967.
(104) Howard, C. J. Kinetic Study of the Equilibrium HO2 + NO ⇋ OH + NO_2 and the Thermochemistry of HO_2. *J. Am. Chem. Soc.* **1980**, *102*, 6937−6941, DOI: 10.1021/ja00543a006.
(105) Litorja, M.; Ruscic, B. A Photoionization Study of the Hydroperoxyl Radical, HO_2, and Hydrogen Peroxide, H_2O_2. *J. Electron Spectrosc. Relat. Phenom.* **1998**, *97*, 131−146, DOI: 10.1016/S0368-2048(98)00264-3.
(106) Lubic, K. G.; Amano, T.; Uehara, H.; Kawaguchi, K.; Hirota, E. The ν_1 Band of the DO_2 radical by Difference Frequency Laser and Diode Laser Spectroscopy: The Equilibrium Structure of the Hydroperoxyl Radical. *J. Chem. Phys.* **1984**, *81*, 4826−4831, DOI: 10.1063/1.447508.
(107) Varandas, A. J. C. On the Stability of the Elusive HO_3 Radical. *Phys. Chem. Chem. Phys.* **2011**, *13*, 15619−15623, DOI: 10.1039/C1CP20791A.
(108) Babikov, D.; Kendrick, B. K.; Walker, R. B.; Pack, R. T.; Fleurat-Lesard, P.; Schinke, R. Metastable States of Ozone Calculated on an Accurate Potential Energy Surface. *J. Chem. Phys.* **2003**, *118*, 6298−6308, DOI: 10.1063/1.1557936.
(109) Varandas, A. J. C. Extrapolation to the Complete-Basis-Set Limit and the Implications of Avoided Crossings: The $X^1\sum_g^+$, $B\ ^1\Delta_g$, and $B'^1\sum_g^+$ States of C_2. *J. Chem. Phys.* **2008**, *129*, 234103 DOI: 10.1063/1.3036115.
(110) Graff, M. M.; Wagner, A. F. Theoretical Studies of Fine-Structure Effects and Long-range Forces: Potential-Energy Surface and Reactivity of $O(^3P)$ + $OH(^2\Pi)$. *J. Chem. Phys.* **1990**, *92*, 2423−2439, DOI: 10.1063/1.457986.
(111) Graff, M. M.; Wagner, A. F. Theoretical Studies of Fine-Structure Effects and Long-Range Forces: Approximating the Reactive Surface of $O(^3P)$ + $OH(^2\Pi)$. *Chem. Phys. Lett.* **1990**, *174*, 287−293, DOI: 10.1016/0009-2614(90)85347-F.
(112) Hirschfelder, J. O.; Curtiss, R. F.; Bird, R. B. *Molecular Theory of Gases and Liquids*; Wiley: New York, 1954.
(113) Clary, D. C.; Werner, H. J. Quantum Calculations on the Rate Constant for the O + OH Reaction. *Chem. Phys. Lett.* **1984**, *112*, 346−350, DOI: 10.1016/0009-2614(84)85755-3.
(114) Slater, J. C.; Kirkwood, K. G. The van der Waals Forces in Gases. *Phys. Rev.* **1931**, *37*, 682−697, DOI: 10.1103/PhysRev.37.682.
(115) Bytautas, L.; Ruedenberg, K. Correlation Energy and Dispersion Interaction in the Ab Initio Potential Energy Curve of the Neon Dimer. *J. Chem. Phys.* **2008**, *128*, 214308 DOI: 10.1063/1.2927302.
(116) Varandas, A. J. C. On the Relation of Dispersion to Induction Energies, Their Damping Functions. Ion-Atom Potentials: the $X^2\sum_g^+$ and $1^2\sum_u^+$ of $H2^+$. *Mol. Phys.* **1987**, *60*, 527−539, DOI: 10.1080/00268978700100341.
(117) Meerts, W. L.; Dynamus, A. Electric Dipole Moments of OH and OD by Molecular Beam Electric Resonance. *Chem. Phys. Lett.* **1973**, *23*, 45−47, DOI: 10.1016/0009-2614(73)89560-0.
(118) Fischer, C. F. Average-Energy-of-Configuration Hartree-Fock Results for the Atoms Helium to Radon. *At. Data Nucl. Data Tables* **1973**, *12*, 87−99, DOI: 10.1016/0092-640X(73)90014-4.
(119) Gray, C. G.; Gubbins, K. E. *Theory of Molecular Fluids*; Oxford University Press: New York, 1984; Vol. *1*.
(120) Chu, X.; Dalgarno, A. Linear Response Time-Dependent Density Functional Theory for van der Waals Coefficients. *J. Chem. Phys.* **2004**, *121*, 4083−4088, DOI: 10.1063/1.1779576.
(121) Vydrov, O. A.; Voorhis, T. V. Dispersion Interactions From a Local Polarizability Model. *Phys. Rev. A* **2010**, *81*,.
(122) Varandas, A. J. C. Accurate Combined-Hyperbolic-Inverse-Power-Representation of Ab InitioPotential Energy Surface for the Hydroperoxyl Radical and Dynamics Study of O + OH Reaction *J. Chem. Phys.*, (in press) DOI: 10.1063/1.4795826.
(123) Woon, D. E.; Dunning, T. H., Jr. Gaussian Basis Sets for Use in Correlated Molecular Calculations. V. Core-Valence Basis Sets for Boron Through Neon. *J. Chem. Phys.* **1995**, *103*, 4572−4585, DOI: 10.1063/1.470645.
(124) Peterson, K.; Dunning, T., Jr. Accurate Correlation Consistent Basis Sets for Molecular Core-Valence Correlation Effects: The Second Row Atoms Al-Ar, and the First Row Atoms B-Ne Revisited. *J. Chem. Phys.* **2002**, *117*, 10548−10560, DOI: 10.1063/1.1520138.
(125) Varandas, A. J. C. Combined-Hyperbolic-Inverse-Power-Representation of Potential Energy Surfaces: A Preliminary Assessment for H_3 and HO_2. *J. Chem. Phys.* **2013**, *138*, 054120 DOI: 10.1063/1.4788912.